Check for updates

Geochemistry, Geophysics, Geosystems

Lithospheric Architecture and Mantle Metasomatism Linked to Iron Oxide Cu-Au Ore Formation: Multidisciplinary Evidence from the Olympic Dam Region, South Australia

R. G. Skirrow[1] (iD)**, S. E. van der Wielen[1]** (iD)**, D. C. Champion[1], K. Czarnota[1], and S. Thiel[2,3]** (iD)

[1]Geoscience Australia, Canberra, ACT, Australia, [2]Geological Survey of South Australia, Adelaide, South Australia, Australia, [3]School of Physical Sciences, The University of Adelaide, Adelaide, South Australia, Australia

Abstract The role of lithospheric architecture and the mantle in the genesis of iron oxide copper-gold (IOCG) deposits is controversial. Using the example of the Precambrian Gawler Craton (South Australia), which hosts the giant Olympic Dam IOCG deposit, we integrate geophysical data (seismic tomography and magnetotellurics) with geological and geochemical data to develop a new interpretation of the lithospheric setting of these deposits. Spatially, IOCG deposits are located above the margin of a mantle lithospheric zone with anomalously high electrical conductivities (resistivity <10 ohm.m, top at ~100–150 km depth), low seismic shear-wave velocities (horizontal component, Vsh < 4.6 km/s), and unusually high ratios of compressional- to shear-wave velocities (Vp/Vsh > 1.80). The high conductivity cannot be explained by water-bearing olivine-rich rock alone. Relatively fertile and metasomatized peridotitic mantle with additional high-Vp/Vs phases, for example, clinohumite, hydrous garnet, and/or phlogopite, could explain the anomalous velocity and conductivity. The top of this high-Vp/Vsh zone marks a midlithospheric discontinuity at ~100–130 km depth that is interpreted to reflect locally orthopyroxene-rich mantle. A sub-Moho zone with high Vp/Vsh at ~40–80 km depth correlates spatially with primitive Nd isotope signatures and arc-related ~1,620–1,610 Ma magmatism and is interpreted as the eclogitic root of a magmatic arc. Mafic volcanics contemporaneous with ~1,590 Ma IOCG mineralization have geochemistry suggesting derivation from subduction-modified lithospheric mantle. We suggest that Olympic Dam formed inboard of a continental margin in a postsubduction setting, related to foundering of previously refertilized and metasomatized lithospheric mantle. Deposits formed during the switch from compression to extension, following delamination-related uplift and exhumation.

1. Introduction

The Olympic Dam Cu-U-Au deposit in South Australia is one of the largest and most valuable ore deposits on Earth, comprising a total resource of 10.4 billion tonnes grading 0.77% Cu, 0.25 kg/t U_3O_8, and 0.32 g/t Au (www.bhp.com). Although Olympic Dam is the archetypal member of the iron oxide copper-gold (IOCG) ore deposit class, an understanding of its genesis and tectonic setting has remained elusive, in part due to concealment of the deposit and much of its host terrane, the Archean-Proterozoic Gawler Craton, by postmineralization basins and regolith. Indeed, the tectonic settings of IOCG deposits globally are poorly understood relative to knowledge of the settings of many other major mineral deposit types. A wide range of settings have been proposed, in part reflecting the ongoing debate on the definitions and characteristics of IOCG deposits. Early models of Fe oxide-Cu-Au-rare earth element (REE) deposits (including Olympic Dam and some magnetite-apatite deposits) suggested anorogenic, intracontinental settings (Hitzman et al., 1992), with later models favoring orogenic and subduction-related continental margin settings (e.g., Hitzman, 2000; Sillitoe, 2003). While considering continental magmatic arcs as key settings for some Phanerozoic IOCG deposits, for Precambrian IOCG deposits, Groves et al. (2010) emphasized the role of mantle plumes in partial melting of previously metasomatized lithospheric mantle in anorogenic, extensional, craton margin settings. Betts et al. (2009) proposed a *plume-modified orogenic* setting that placed the Australian Mesoproterozoic IOCG deposits (including those in the Gawler Craton and Cloncurry district) within a back-arc environment above a subducting oceanic plateau and hot spot (Betts et al., 2009). Distal back-arc and postsubduction, extensional settings were proposed for those subtypes of IOCG deposits described as magmatic-hydrothermal by Richards and Mumin (2013). An

alternative setting involving removal of lithospheric mantle was proposed by Skirrow (2010) for IOCG deposits in the Gawler Craton and Curnamona Province of South Australia.

Several studies have proposed either a direct or indirect role of mantle-derived magmas or rocks in the formation of IOCG deposits (e.g., Groves et al., 2010; Hitzman, 2000; Johnson & McCulloch, 1995; Skirrow, 1999). Whereas most of these studies based their conclusions on geochemical, radiogenic isotopic, and geological constraints, none have attempted to relate the locations of IOCG deposits to mapped spatial variations in mantle architecture and composition. Indeed, there have been few studies of any ore deposit types that consider such spatial associations, and these have focused mainly on diamonds (e.g., Jones et al., 2009; Snyder, 2008; Snyder et al., 2014) and Ni-Cu-PGE deposits (e.g., Begg et al., 2010). Steadily improving regional- to continental-scale seismic tomographic and magnetotelluric (MT) data sets, such as the AusLAMP survey of Australia (www.ga.gov.au/about/projects/resources/auslamp), offer the opportunity to better understand the spatial and genetic relationships between mantle architecture and composition and major ore deposits.

Here we utilize recent advances in geophysical (passive seismic tomographic and MT) imaging of the lithosphere in part of southern Australia as a three-dimensional (3-D) framework for integrating the available geological, geochemical, geochronological, and isotopic data sets. The interpreted lithospheric architecture and variations in mantle composition form the foundation for development of a new model of the evolution of the lithosphere hosting major IOCG deposits in the Gawler Craton. Combined with an understanding of IOCG ore-forming processes, this spatial and temporal framework enables predictions of new regions with high potential for major IOCG deposits.

We argue that the multidisciplinary data image a Paleoproterozoic to early Mesoproterozoic convergent margin that developed along an Archean continental ribbon and further propose that lithospheric mantle beneath the Archean-Proterozoic crust was substantially modified. Mantle-derived magmatism is viewed as the product of lithospheric thinning, possibly localized and triggered by foundering of thickened, previously refertilized and metasomatized, lithospheric mantle. In this model the mantle magmas, guided by trans-lithospheric weak zones, ultimately drove crustal melting and development of giant hydrothermal systems that produced IOCG mineralization including the giant Olympic Dam deposit. The multidisciplinary imaging of lithospheric architecture and new tectonic setting proposed in this study provide a more robust framework for deciphering the settings and spatial controls of IOCG deposits, and for their exploration targeting, in southern Australia and globally.

2. Geologic Setting

The Olympic Dam Cu-U-Au and other IOCG deposits in the South Australian crustal element occur within the Olympic Cu-Au Province (Skirrow et al., 2002; Skirrow et al., 2007) along the eastern margin of the Mesoarchean to Mesoproterozoic Gawler Craton (Figure 1). Small IOCG deposits are also present in the western part of the Paleoproterozoic to Mesoproterozoic Curnamona Province, which, at upper crustal levels at least, is separated from the Gawler Craton by Neoproterozoic sequences of the Adelaide Rift Complex (Figure 1). The Gawler Craton comprises several domains, defined by their lithostratigraphic as well as gravity and magnetic characteristics (Ferris et al., 2002). However, published seismic tomography data for the mantle, described further below, show evidence of contiguity between sub-Gawler Craton and sub-Curnamona Province lithospheric mantle.

The Gawler Craton records a long and complex evolution commencing in the Mesoarchean, and with cratonization in the early Mesoproterozoic (Figures 1 and 2; Hand et al., 2007; Reid, 2017; Reid & Hand, 2012). The oldest identified unit is the ~3.15 Ga Cooyerdoo Granite in the southeastern Gawler Craton (Fraser et al., 2010). All other known Archean rocks in the Gawler Craton occur within the Sleaford Complex in the south and the Mulgathing Complex in the north. These comprise ~2,560–2,500 Ma supracrustal and intrusive rocks (Hand et al., 2007; Reid & Hand, 2012; Reid, 2017). Komatiites (~2,520 Ma; Hoatson et al., 2005) are present within the Harris Greenstone Belt in the central Gawler Craton (Figure 1), where juvenile calc-alkaline volcanics are also present and are interpreted to have formed in an active subduction environment (Swain et al., 2008). The Mesoarchean and Neoarchean rocks were deformed and metamorphosed during the Sleafordian orogeny at ~2,480–2,420 Ma (Figure 2; Hand et al., 2007; Reid, 2017; Reid & Hand, 2012).
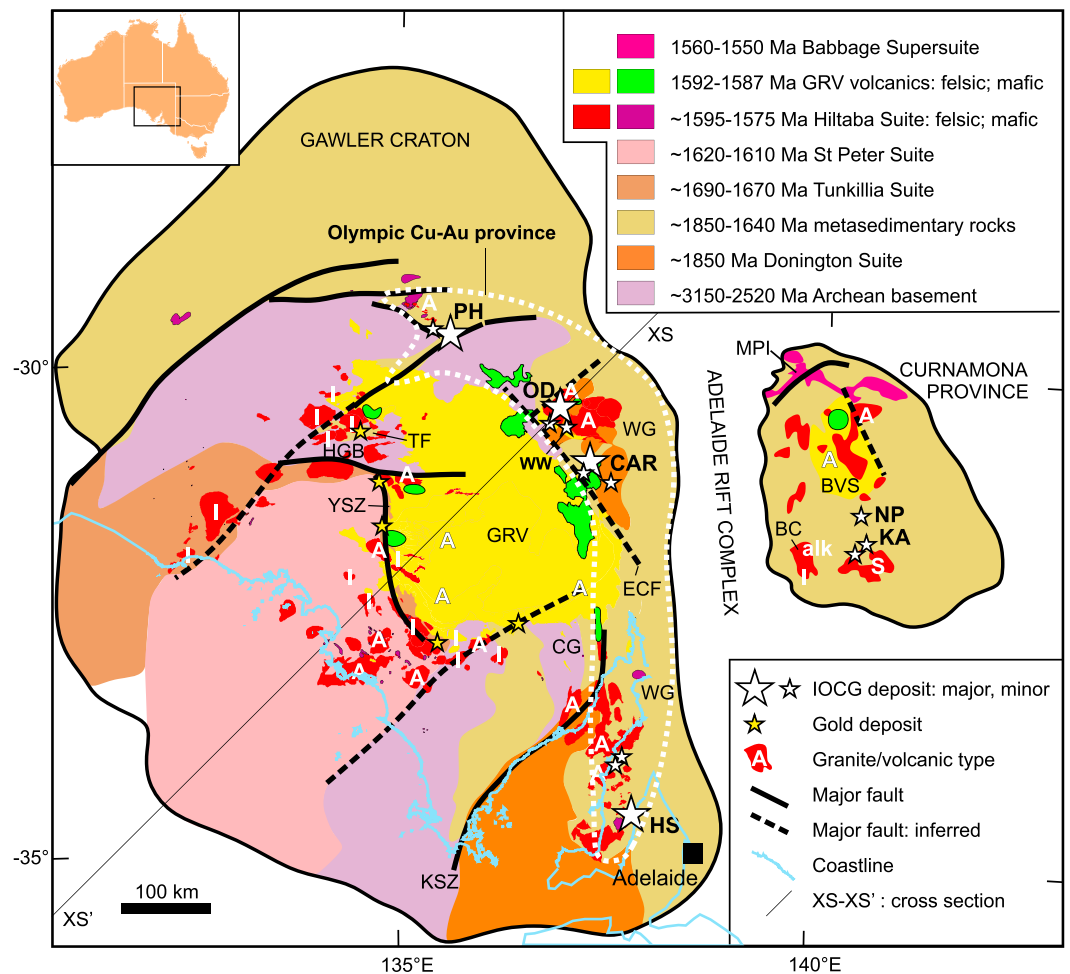
Figure 1. Archean to early Mesoproterozoic interpreted geology of the Gawler Craton and Curnamona Province, showing locations of IOCG and Au deposits, and position of cross section XS-XS'. Granite and volcanic petrogenetic types (A, I, and S) are from Budd (2006). Geology based on Hand et al. (2007) and the pre-Pandurra Formation geology of Cowley (2008). Olympic Cu-Au province boundary (dash white line) modified from Skirrow et al. (2007). Abbreviations: BC, Billeroo Complex; CAR, Carrapateena deposit; CG, Cooyerdoo Granite; ECF, Elizabeth Creek Fault; GRV, Gawler Range Volcanics; HGB, Harris Greenstone Belt; HS, Hillside deposit; KA, Kalkaroo deposit; KSZ, Kalinjala Shear Zone; MPI, Mt Painter Inlier; NP, North Portia deposit; OD, Olympic Dam deposit; PH, Prominent Hill deposit; TF, Tarcoola Formation; WG, Wallaroo Group; YSZ, Yarlbrinda Shear Zone.

Following localized felsic magmatism at ~2,000 Ma a series of basins developed between ~1,870 Ma and ~1,740 Ma within, and on the eastern and northern margins of, the Archean core of the Gawler Craton. This basin formation was punctuated by felsic to mafic intrusive magmatism of the Donington Suite at ~1,850 Ma during the medium- to high-metamorphic grade Cornian Orogeny. The ~1,760–1,740 Ma Wallaroo Group is one of several Paleoproterozoic basin successions along the eastern margin of the craton and constitutes one of the main host units for IOCG mineralization in the Olympic Cu-Au Province. The Kimban orogeny at ~1,730–1,710 Ma was followed by a period of igneous intrusive activity from ~1,690 to ~1,580 Ma, with few preserved, coeval, basin rocks (e.g., Tarcoola Formation, ~1,660 Ma; Fanning, 1990). Intrusive suites include the 1,690–1,670 Ma I-type Tunkillia Suite, which forms an arcuate belt in the central Gawler Craton and has geochemical characteristics suggesting continental magmatic arc affinities (Ferris et al., 2002). Rift basins developed in the Curnamona Province at ~1,730 Ma with sedimentation continuing to ~1,640 Ma (Willyama Supergroup; Fitzherbert & Downes, 2017). The volcanic suites associated with these basins in both the Gawler Craton and Curnamona Province are dominantly bimodal (Fitzherbert & Downes, 2017; Hand et al., 2007, and references therein).
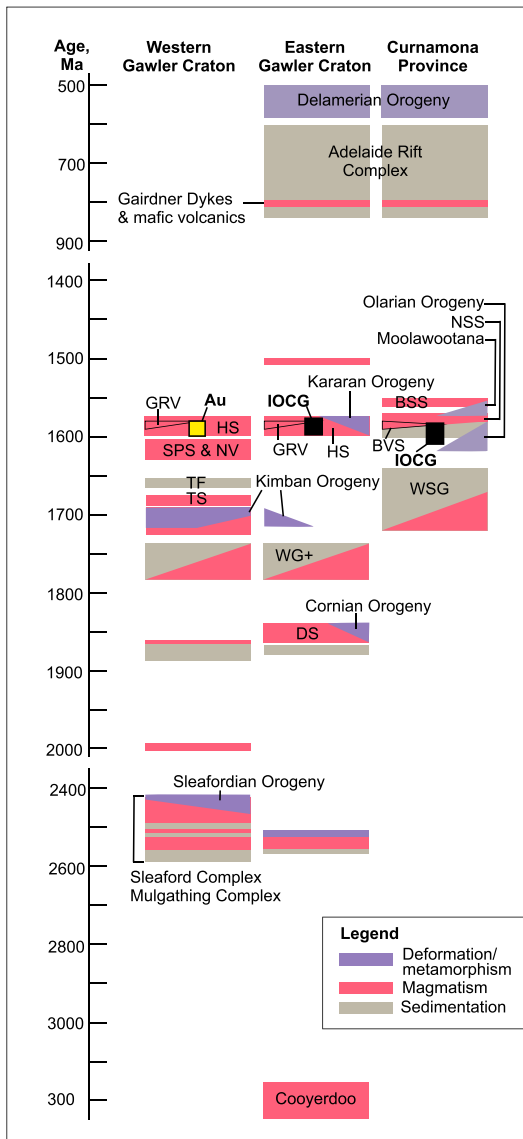
Figure 2. Time-space diagram for the Gawler Craton and Curnamona Province. The columns for the western and eastern Gawler Craton represent regions to the west and east, respectively, of the Kalinjala Shear Zone (Figure 1). Adapted from Reid and Hand (2012) with addition of Curnamona Province information from Fitzherbert and Downes (2017) and ages of IOCG and gold deposits (Fraser et al., 2007; Skirrow et al., 2007). Ages of Olarian Orogeny and Kararan Orogeny modified according to Forbes et al. (2007) and Hand et al. (2007), respectively. Abbreviations: BSS, Babbage Supersuite; BVS, Benagerie Volcanic Suite; DS, Donington Suite; GRV, Gawler Range Volcanics; HS, Hiltaba Suite; NSS, Ninnerie Supersuite; NV, Nuyts Volcanics; SPS, St Peter Suite; TF, Tarcoola Formation; TS, Tunkillia Suite; WG+, Wallaroo Group and other Paleoproteroic basins; WSG, Willyama Supergroup.

These events were succeeded in the west and south of the Gawler Craton by emplacement of the ~1,630 Ma felsic Nuyts Volcanics and then felsic and mafic-ultramafic intrusions of the St Peter Suite at ~1,620–1,610 Ma. Geochemical and isotopic compositions of the St Peter Suite have been interpreted as indicative of a subduction-related magmatic arc or back-arc setting (Ferris et al., 2002; Swain et al., 2008; Wade, 2012) or remelting of previously subduction-modified mantle (Hayward & Skirrow, 2010). Deformation associated with the St Peter Suite may have occurred in a compressional, plate margin, setting (Hand et al., 2007).

The felsic-dominated intrusive Hiltaba Suite and Gawler Range Volcanics (GRV) magmatic event between ~1,595 and ~1,575 Ma affected much of the Gawler Craton as well as parts of the Curnamona Province where the equivalents are known as the Ninnerie Suite and Benagerie Volcanic Suite (BVS), respectively (Figure 2; e.g., Wade et al., 2012). This magmatic event temporally overlaps with the formation of the IOCG ore-forming systems. The Hiltaba-GRV magmatic system represents one of the largest felsic-dominated igneous events in the world, with preserved areas in the Gawler Craton alone covering >25,000 km^2 and attaining thicknesses of ~1.5 km (Hand et al., 2007). Wade et al. (2012) suggested that the total volume of Gawler and Curnamona magmatism of this age was ~1.1×10^5 km^3. The Hiltaba Suite and comagmatic GRV have been divided into four supersuites based on major and trace element compositions (Budd, 2006): alkali A-type, alkali-calcic A-type, moderately fractionated I-type, and strongly fractionated I-type (Figure 1). Although dominated by felsic compositions, both the granite-dominated Hiltaba Suite and dacite-rhyolite-dominated GRV contain important mafic igneous rock components represented predominantly by gabbro, dolerite, and basalt to basaltic andesite. Volumetrically minor rocks of intermediate (andesitic and dioritic) composition are also present, as are rare ultramafic intrusives (at the Olympic Dam deposit: Reeve et al., 1990; Johnson & Cross, 1995; Huang et al., 2016; *picrite* at the Wirrda Well deposit: Huang et al., 2016) and Na- and K-alkaline intrusives (Billeroo Complex, Rutherford et al., 2007). The Hiltaba Suite granites and temporally associated mafic-ultramafic-alkaline intrusive rocks were emplaced over a broad period from ~1,595 to ~1,575 Ma, whereas the GRV, BVS, and equivalent volcanics in the Olympic Dam region were erupted over a relatively short period between ~1,595 and ~1,587 Ma across both the Gawler Craton and Curnamona Province (Figure 2; Wade et al., 2012; Jagodzinski et al., 2016).

Whereas Hiltaba Suite and GRV magmatism had been widely considered to have developed in an anorogenic or extensional setting (e.g., Creaser, 1996; Giles, 1988), more recent geochronological and geological data demonstrate that the early part of this magmatism was in part synchronous with the compressional Olarian orogeny in the Curnamona Province and was partly coeval with deformation and metamorphism in the Gawler Craton (Figure 2; Hand et al., 2007; Reid & Hand, 2012). Northwest-southeast directed shortening in the Curnamona Province was associated with crustal anatexis and low-pressure high-temperature metamorphism, which may have commenced as early as ~1,619 Ma and peaked at ~1,600 Ma (Forbes et al., 2007). Although the timing, kinematics, and metamorphic conditions of the coeval orogeny in the Gawler Craton remain relatively poorly constrained, there is field evidence for emplacement of early Hiltaba Suite intrusions synchronous with deformation whereas later phases generally are less deformed or undeformed (Hand et al., 2007; Reid & Hand, 2012). The bimodal GRV is largely flat-lying and undeformed and includes local sedimentary facies up to several hundred meter thick (e.g., intercalated with Roopena Basalt,

McAvaney & Wade, 2015; Curtis et al., 2018). These relationships, and seismic reflection evidence of GRV-filled half-graben (Carr et al., 2010), support previous suggestions of an extensional kinematic regime during GRV eruption. Thus, there is evidence of a switch from compressional orogenesis at ~1,600–1,595 Ma to extension at ~1,595–1,587 Ma across both the Gawler Craton and Curnamona Province (Hayward & Skirrow, 2010; Skirrow, 2010). It was during this switch that the major IOCG ore-forming systems developed.

Subsequent volumetrically minor magmatism, deformation, and metamorphism during the Kararan orogeny (1,570–1,540 Ma; Hand et al., 2007) was largely restricted to the north-central and western parts of the Gawler Craton (e.g., Coober Pedy Ridge and Fowler Domain) and also occurred in the northernmost Curnamona Province (e.g., Mt Painter Inlier and Mt Babbage Inlier). Apart from localized reactivation of terrane-scale shear zones during the period 1,470–1,450 Ma (Fraser & Lyons, 2006), the Gawler Craton and Curnamona Province remained relatively stable until ~830 Ma when rifting commenced between the two provinces in association with emplacement of the Gairdner large igneous province (Figure 2; Wingate et al., 1998). The doleritic Gairdner Dyke Swarm traverses the eastern margin of the Gawler Craton, with the causative plume head inferred to have been once present to the southeast of the Gawler Craton (now possibly located in a separate continental fragment following the breakup of the Rodinia supercontinent; Zhao et al., 1994). The Delamerian Orogeny at ~500 Ma (Figure 2) affected large parts of southeastern Australia including the Neoproterozoic basinal sequences of the Adelaide Rift Complex as well as the southern Curnamona Province and resulted in minor felsic plutonism in the northern Curnamona Province. Breakup of the Gondwana supercontinent commenced in the Jurassic, resulting in rifting of the Mawson continent along what is now the southern margin of the Gawler Craton; remnants of the Mawson continent occur in Antarctica. Several clusters of alkaline igneous rocks, including diamond-bearing kimberlites, were emplaced during the Jurassic and Permian in the southern Gawler Craton and along its southeastern margin within the Adelaide Rift Complex (Cooper & Morris, 2012; Gaul et al., 2003; Tappert et al., 2011).

3. IOCG and Gold Deposits

IOCG deposits occur within three districts in the eastern Gawler Craton, forming the Olympic Cu-Au Province, and are also present in the Olary Domain in the western Curnamona Province (Figures 1 and 2). Available geochronological and relative timing constraints indicate that Fe oxide-associated Cu-Au $\pm$ U $\pm$ REE mineralization and hydrothermal alteration developed between ~1,595 and ~1,575 Ma in the Gawler Craton (Bowden et al., 2017; Ciobanu et al., 2013; Conor et al., 2010; Johnson & Cross, 1995; Reeve et al., 1990; Reid et al., 2013; Skirrow et al., 2002; Skirrow et al., 2007). In the Curnamona Province small Fe oxide-associated Cu-Au $\pm$ Mo deposits appear to have formed somewhat earlier than in the Gawler Craton, at ~1,610–1,605 Ma (molybdenite Re-Os ages), although relative timing constraints suggest syn-Olarian orogeny Fe-Cu-Au-Mo hydrothermal activity (Figure 2; Skirrow et al., 2000; Williams & Skirrow, 2000). These constraints are supported by imprecise U-Pb ion probe ages for allanite and monazite associated with Cu sulphides (1,590 $\pm$ 36 Ma, 1,596 $\pm$ 19 Ma, Kalkaroo deposit; Reid & Jagodzinski, 2013). In all IOCG districts in the Gawler Craton and Curnamona Province there is a consistent pattern of paragenetically early, relatively high-temperature, hydrothermal magnetite-rich alteration with or without minor Cu-Au mineralization, overprinted by hematite-rich lower temperature alteration and associated Cu-Au $\pm$ U $\pm$ REE mineralization (Belperio et al., 2007; Conor et al., 2010; Reeve et al., 1990; Schlegel & Heinrich, 2015; Skirrow et al., 2002; Williams & Skirrow, 2000). In many cases the early sodic (albite), sodic-calcic (albite-actinolite$\pm$diopside), and magnetite-rich potassic (K-feldspar or biotite) alteration with generally minor Cu-Au $\pm$ Mo mineralization formed during brittle-ductile deformation within shear zones (e.g., Moonta-Wallaroo district; Olary district). In contrast, later hematitic Cu-Au $\pm$ U $\pm$ REE mineralization and sericite-chlorite $\pm$ carbonate alteration occurs in brittle deformation structures such as breccias and fault zones. Although the kinematics of deformation during IOCG mineralization have yet to be determined precisely, the relative and absolute timing constraints are consistent with a model in which early magnetite-rich IOCG alteration developed during regional compressional deformation (i.e., syn-Olarian orogeny), whereas the major Cu-Au $\pm$ U $\pm$ REE ore-forming event(s) occurred when tectonism switched to an extensional or transtensional regime, roughly coeval with emplacement of the GRV (Hayward & Skirrow, 2010; Skirrow, 2010).

In contrast to the Cu- and Fe-oxide-rich IOCG deposits in the Olympic Cu-Au Province and Curnamona Province, Au deposits lacking significant Cu or Fe oxides are present in the central Gawler Craton (Figure 1;
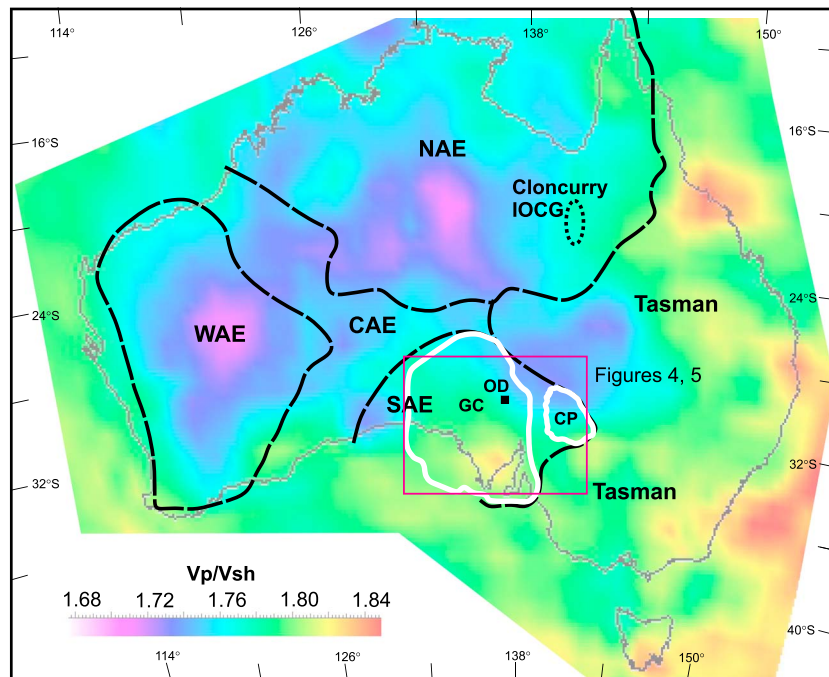
Figure 3. Vp/Vsh map of Australia at ~160 km depth, representing the ratio of *P* wave (Vp) and *S* wave (horizontal component, Vsh) velocities. Extract from 3-D model (supporting information; see also Appendix A for data sources). Outlines of the Gawler Craton (GC) and Curnamona Province (CP), shown as white lines. Outlines of major Archean-Proterozoic crustal elements (WAE, West Australian element; SAE, South Australian element; NAE, North Australian element) and the Paleozoic Tasman element from Champion (2013). Locations of the Olympic Dam deposit (OD) and the Cloncurry IOCG province are also indicated.

Ferris & Schwarz, 2003; Budd & Skirrow, 2007). Although known resources are small, these deposits are metallogenetically important because they are thought to have formed broadly synchronously with the IOCG deposits to the east, based on relative timing relationships and ^{40}Ar-^{39}Ar dating of associated sericitic alteration (Figure 2; Fraser et al., 2007). The origins of the Au-only deposits, and reasons for the differences with the coeval IOCG deposits, have been unclear. Both orogenic and intrusion-related models are plausible (Budd, 2006; Budd & Skirrow, 2007; Ferris & Schwarz, 2003).

4. Spatial Correlations and Interpretation of Lithospheric Architecture

4.1. Data Sets

A wide range of geophysical, geological, isotopic, and geochemical data were utilized and integrated within 2-D and 3-D models, using GOCAD® software. Data types and sources are described in the Appendix A and include seismic tomographic (velocity) data based on the mantle component of the AuSREM data set (Kennett et al., 2013); MT data from Thiel and Heinson (2013) and Robertson et al. (2016); whole-rock geochemistry of mafic igneous rocks, neodymium isotope data, and geological and geochronological information compiled from various sources (Appendix A); and data from mantle xenoliths and xenocrysts (Gaul et al., 2003; Tappert et al., 2011). Additionally we have derived several new data sets from the public domain data, as described in Appendix A. These include a new 3-D velocity data set that was created by combining the compressional or *P* wave velocity (Vp) model of Sun and Kennett (2016) with the shear wave velocity (*S* wave, Vs) data from Kennett et al. (2013). A depth slice of the resultant continental 3-D model of the Vp/Vs ratio is shown in Figure 3, utilizing the horizontal component of the shear wave velocity (Vsh). A 3-D model of the geophysical data, integrated with several of the other data sets, is available in the supporting information.

Several remarkable and significant spatial correlations emerge from the integration of the 3-D seismic velocity and electrical conductivity data with the basement geology, mafic whole-rock geochemistry, neodymium isotope, and mantle xenolith data. Key results are described below.
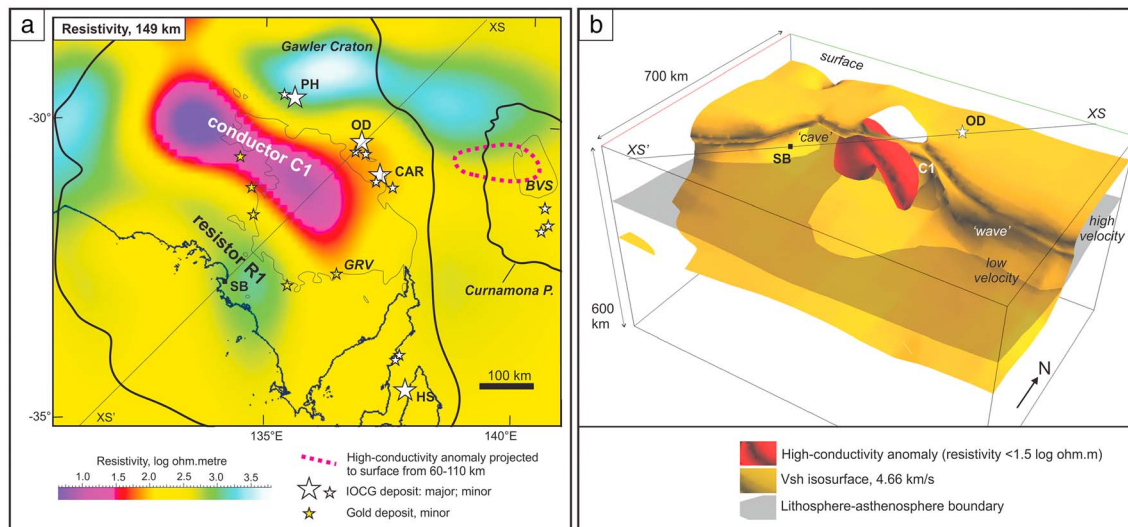
Figure 4. (a) Variation in electrical resistivity at a depth of 150 km, extracted from a 3-D model of magnetotelluric data of the Gawler Craton (Thiel & Heinson, 2013; van der Wielen et al., 2016; see also supporting information). Outline of conductivity anomaly beneath part of the Curnamona Province from Robertson et al. (2016). The line XS-XS′ marks the cross section in Figure 6. Conductivity and resistivity anomalies are labeled C1, R1, (b) Oblique view (to northwest and downwards) of 3-D model, showing high-conductivity anomaly C1 in relation to a representative Vsh isovelocity surface extracted from the AuSREM dataset of Kennett et al. (2013) and the lithosphere-asthenosphere boundary of Czarnota et al. (2014). Note position of anomaly C1 in the *cave* and fold of the *wave* of the isovelocity surface. Abbreviations: BVS, Benagerie Volcanic Suite; CAR, Carrapateena deposit; GRV, Gawler Range Volcanics; HS, Hillside deposit; OD, Olympic Dam deposit; PH, Prominent Hill deposit; SB, Streaky Bay town.

4.2. Correlated High-Conductivity and Low-Velocity Mantle Domains

An extensive northwest-southeast to east-west trending zone of high electrical conductivity (with resistivity as low as 1.3 ohm.m) was identified by Thiel and Heinson (2013) in the midlithospheric to deep-lithospheric mantle of the Gawler Craton (Figure 4a). Three-dimensional rendering of the MT data shows that the top of this body (as defined by a 10 ohm.m resistivity isosurface) lies at depths of ~100–150 km (Thiel & Heinson, 2013; van der Wielen et al., 2016; supporting information; Gawler MT anomaly C1). Long-period MT data for a region covering the Curnamona Province and parts of the Adelaide Rift Complex also define a mantle lithosphere-hosted zone of high conductivity that connects with complex-shaped high-conductivity zones in the crust of the Curnamona Province and surrounds (Robertson et al., 2016). Collectively, the MT data show that the mantle lithosphere-hosted high-conductivity zone C1 (as defined by 10 ohm.m isosurface) in the Gawler Craton extends eastward toward the mantle-hosted anomaly beneath the Curnamona Province, suggesting a (semi)contiguous zone of high conductivity (see supporting information, 3-D model).

Thiel and Heinson (2013) noted that lithosphere in the central Gawler Craton is characterized by relatively low shear-wave velocities. Three-dimensional visualization by van der Wielen et al. (2016) and in the present study (supporting information) confirms and refines this observation. The Gawler MT anomaly C1 occupies mantle with an average Vsh data (horizontal component of shear-wave velocity) of 4.61 km/s and minimum Vsh of 4.59 km/s. Figure 4b shows a Vsh isovelocity surface *wrapping* around the highly conductive zone. The wave-like form of the isovelocity surface represents part of a strong horizontal gradient in shear-wave velocity, which is evident in the plan view shown in Figure 5a at a depth of 150 km. A similar shaped embayment of relatively low Vp coincident with the high-conductivity anomaly C1 is evident in the ~160 km depth slice shown in Figure 5b.

The horizontal gradients in Vsh, Vp, and Vp/Vsh (Figures 5a–5c) form an arcuate zone bounding a relatively low-Vsh domain occupying the midlithosphere in the southern and central parts of the Gawler Craton, flanked to the northeast and northwest by higher Vsh velocity domains. In our 3-D model, the Vsh isosurfaces in the midlithosphere show S-shaped forms in cross section (Figures 6a and 6b), creating *wave* and *cave-like* features in three dimensions where the isosurfaces are most strongly overturned, which encloses low-Vsh mantle that plunges northwest from the central Gawler Craton into the northern part of the craton. This cave-like 3-D geometry is evident in both the Vsh and Vsv data (vertical component of *S* wave velocity; see
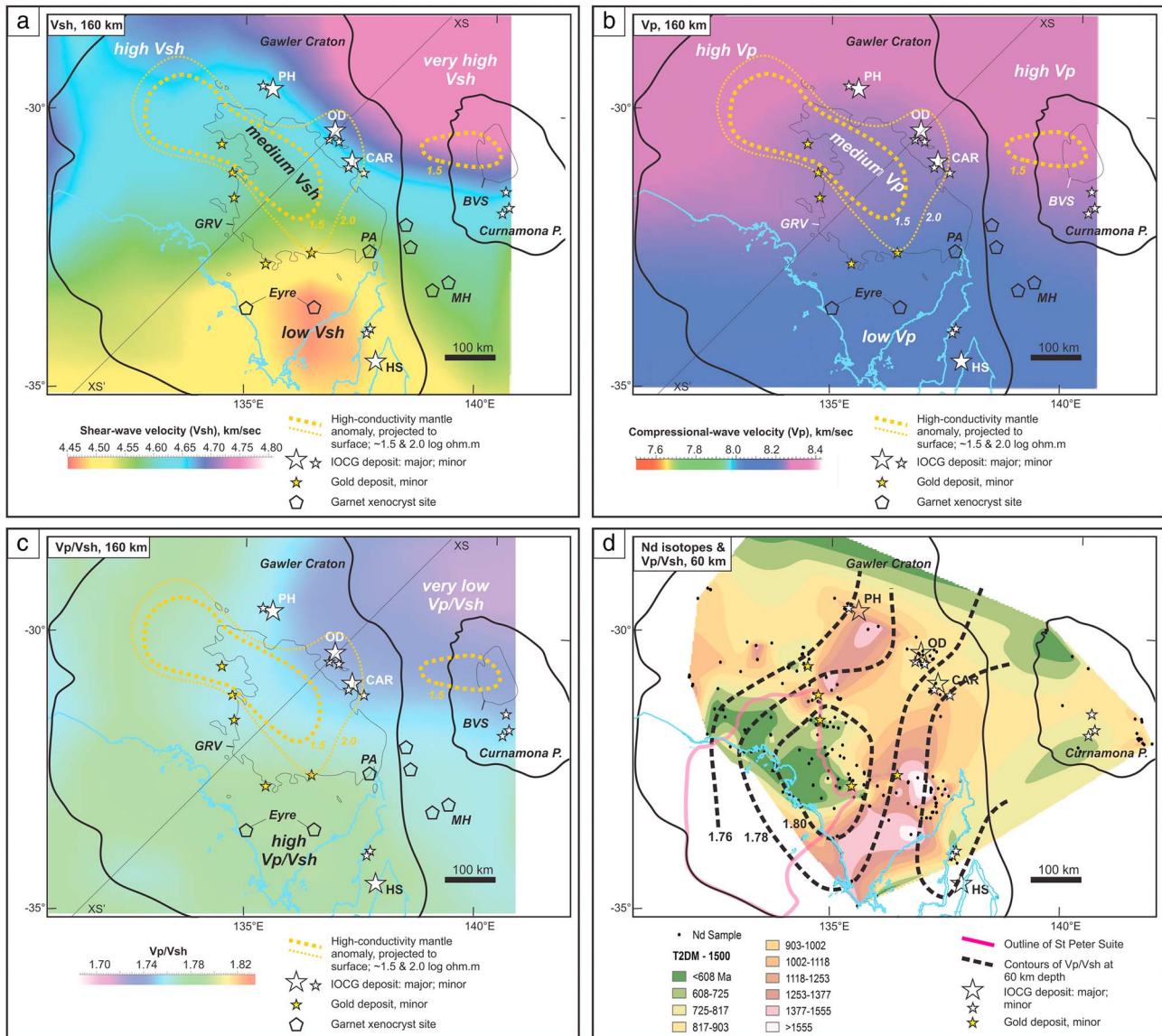
Figure 5. Maps of geophysical and isotopic data of the Gawler Craton and Curnamona Province, in relation to locations of IOCG and Au deposits, Gawler Range Volcanics (GRV), Benagerie Volcanic Suite (BVS), cross section XS-VS' (Figure 6), outlines of MT electrical conductivity anomalies with resistivity contours of ~1.5 and ~2.0 log ohm.m (~32 and ~100 ohm.m) from Thiel and Heinson (2013) and Robertson et al. (2016) projected from ~60–150 km depth to surface, and locations of mantle-derived garnet xenocryst and xenolith samples from Jurassic and Permian alkaline intrusive rocks (Gaul et al., 2003; Tappert et al., 2011). (a) S wave velocity (horizontal component, Vsh) at ~160 km depth. (b) P wave velocity (Vp) at ~160 km depth. (c) Vp/Vsh at ~160 km depth. (d) Neodymium isotope two-stage depleted mantle model ages (T_{2DM}) of ~1630–1575 felsic igneous whole-rock samples (locations shown as small dots), contoured for *residence time* at 1,500 Ma ($T_{2DM\ (1500)}$). Shorter *residence times*, that is, average younger crust, are shown in green whereas very old Archean crust is shown in shades of pink and white. Also shown are selected contours of Vp/Vsh at shallow depth (~60 km) in the upper mantle, and the outline of the ~1,620–1,610 Ma St Peter Suite mafic-felsic intrusive rocks. Note the correlation between short residence times in Nd isotope data, high Vp/Vsh, and the St Peter Suite. Neodymium isotope data are from the compilation of Champion (2013) supplemented by data from Stewart and Foden (2003). Other abbreviations: CAR, Carrapateena deposit; HS, Hillside; MH, Monk Hill mantle xenocryst and xenolith site, OD, Olympic Dam deposit; PA, Port Augusta mantle xenocryst site, PH, Prominent Hill deposit. See Appendix A for sources of geophysical data.

contours in Figure 6b, and supporting information, 3-D model). The cross sections shown in Figures 6a and 6b illustrate the same correlations between S wave velocity and the conductivity variations, with the high-conductivity zone situated within a *wave-like* inflexion in the Vsh and Vsv velocity contours. It is notable that the northwest-southeast trend of the C1 MT anomaly in the Gawler Craton is subparallel to, and broadly coincident with, the northwest-southeast trending part of the gradient in Vp/Vsh shown in Figure 5c. The strong spatial correlation of the highest conductivities with the low-Vsh *cave*-like part of the
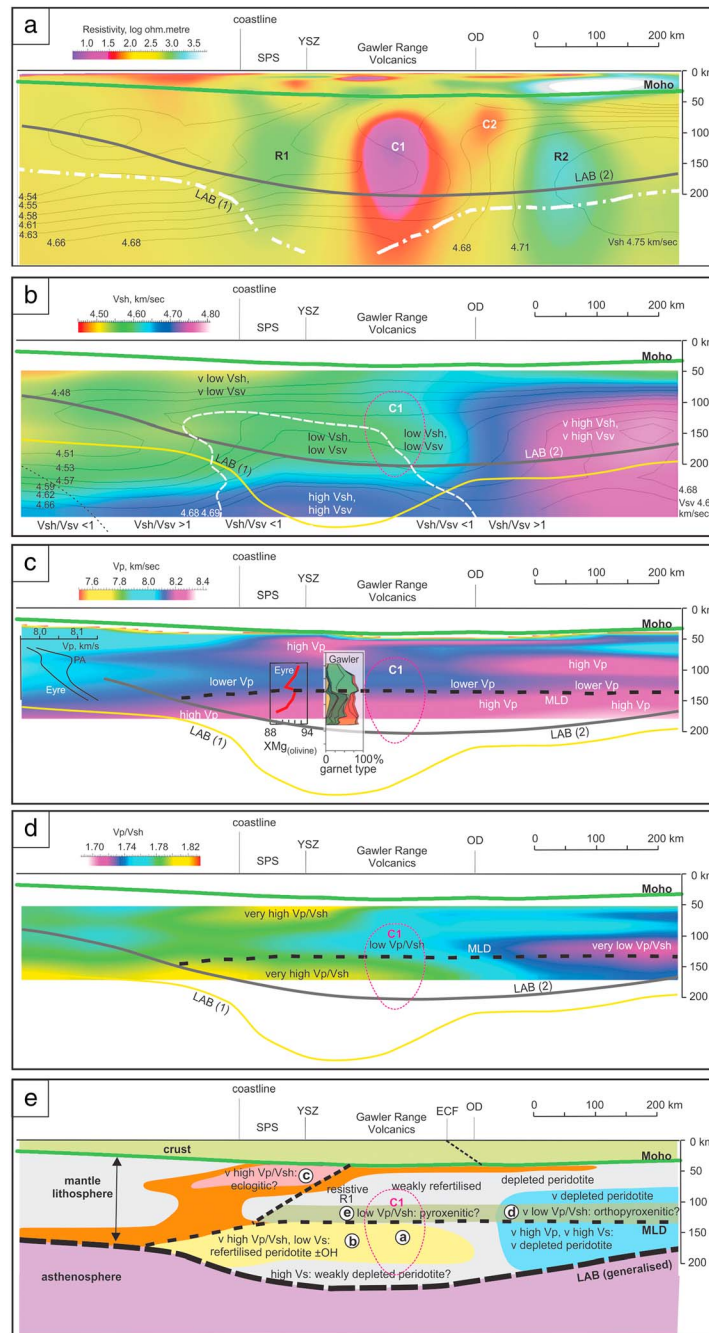
Figure 6. Cross sections of Gawler Craton and surrounding lithosphere along cross-section line XS-XS' (location in Figures 1, 3, and 4). The locations of the Olympic Dam deposit (OD), Gawler Range Volcanics, Yarlbrinda Shear Zone (YSZ), St Peter Suite (SPS), and coastline at Streaky Bay are shown in each panel. Also shown are the Moho (AusMoho, Kennett et al., 2011), and the lithosphere-asthenosphere boundaries of Czarnota et al. (2013) (LAB1) and Kennett et al. (2013) (LAB2). The electrical resistivity/conductivity anomaly C1 is outlined in panels (b)–(e) for a resistivity value of ~1.5 log ohm.m (~32 ohm.m). (a) Electrical resistivity from inversion of magnetotelluric data (Thiel & Heinson, 2013), and contours of Vsh (at 10th-percentile intervals, from data of Kennett et al., 2013), extracted from 3-D models. Note the *wrapping* of velocity contours around the low-resistivity (high-conductivity) zone at ~100–200 km depth. Anomalies C1, C2, and R1 as in Figure 3. (b) S wave velocity (horizontal component, Vsh) with contours of the vertical component of S wave velocity (Vsv); note the midlithospheric domain of relatively low Vsh (4.58–4.63 km/s) enclosing the high-conductivity C1 anomaly. The dashed white line represents Vsh = Vsv; note the region with Vsh < Vsv in the central Gawler Craton, indicating different anisotropy to that of surrounding lithosphere. (c) P wave velocity (Vp). Also shown are two profiles of garnet xenocryst-based compositional variations (center-left: Mg/(Mg + Fe) of olivine at the Eyre location, to south of the cross section; middle-right: proportions of garnets from different types of mantle of the Gawler Craton, from Gaul et al., 2003). At left of the panel are profiles of Vp at the Eyre and Port Augusta (PA) kimberlite sites (locations shown in Figure 5). (d) Vp/Vsh variations; note the inferred MLD at the transition from higher to lower Vp/Vsh. (e) Interpreted present-day lithospheric architecture and mantle compositional domains, based on velocity characteristics (using the calculator of Abers & Hacker, 2016; see text), electrical conductivity, and garnet xenocryst-based constraints. OH = presence of water-bearing minerals.

wave in seismic tomography data is suggestive of a related cause of both the conductivity and velocity variations in this region, although this relationship is not apparent in the available data for the Curnamona Province. In this latter region the mantle-hosted high-conductivity anomaly occurs within relatively high-Vsh, high-Vp mantle, and is elongated subparallel to, but to the north of, the strong velocity gradient. Seismic tomographic data with finer spatial resolution are required to further test the relationships described above.

The Olympic Dam, Prominent Hill, and Carrapateena IOCG deposits lie along a roughly linear northwest-southeast trend immediately to the north of, and parallel to, the northeastern margin (projected to surface) of the high-conductivity MT anomaly C1 (Figure 4a). These deposits are also situated directly above the strong horizontal gradient between a high-Vsh and low-Vp/Vsh domain to northeast and the low-Vsh high Vp/Vsh domain (at ~160 km depth; Figures 5 and 6) in the central Gawler Craton. Both the Vsh and Vsv values for midlithospheric mantle of the central Gawler Craton are significantly lower than those characterizing the lithospheric mantle of much of the Archean Yilgarn Craton (Kennett et al., 2013), as reflected in the Vp/Vsh values (Figure 3). On the other hand, relatively high Vsh, high Vp, and low Vp/Vsh values of the broad domain to the northeast of the Olympic Dam deposit (Figures 5a–5c) are more typical of such highly depleted lithospheric mantle (Figure 3).

4.3. High-Vp/Vsh Upper Mantle Domains, Primitive Nd Isotope Ratios, and St Peter Suite

A second set of robust spatial correlations are evident from the 3-D models of Vsh, Vp, and Vp/Vsh when compared to geological, geochemical, neodymium isotopic, MT, and mantle xenolith data. The complex 3-D structure of Vp/Vsh variations shows a striking *mushroom*-shaped zone of very high Vp and Vp/Vsh values (up to 1.83) extending from the shallowest levels of the mantle velocity model (50 km) to depths of ~70–80 km in the mantle lithosphere, situated beneath the ~1,620–1,610 Ma St Peter Suite in the southwest part of the Gawler Craton (Figures 6c and 6d). The spatial extent of this high-Vp/Vsh zone in the uppermost mantle closely matches the known distribution of the St Peter Suite and, moreover, corresponds well with a domain of relatively primitive Nd isotope compositions (i.e., high $\varepsilon_{Nd(i)}$ values) mapped in St Peter Suite and Hiltaba Suite whole-rock felsic igneous samples (Figure 5d). The two-stage depleted mantle (T_{2DM}) model ages were calculated at 1,500 Ma (i.e., T_{2DM}-1500) from the data of Champion (2013) with additional published data (Stewart & Foden, 2003). These results indicate that the crustal sources of the St Peter Suite and Hiltaba Suite in the southwestern Gawler Craton represent a region characterized by extensive relatively juvenile crustal growth, as recognized by Swain et al. (2008), that is, the crust in this region was largely/wholly generated much more recently than in many other parts of the Gawler Craton (which have much larger T_{2DM}-1500 model ages; Figure 5d). Although this juvenile signature has been known for some time and has been used to support an argument for a subduction-related origin for the St Peter Suite (Champion, 2013; Swain et al., 2008), the lithospheric mantle roots of this magmatic system have not been previously recognized.

The *stalk* of the high-Vp/Vsh mushroom extends downward (and shifts south-eastward with depth) through the midlithospheric mantle, evidently joining a deep and broad zone of similarly anomalous high-Vp/Vsh. Variations of Vp/Vsh at ~160 km depth in plan view are shown in Figure 5c, whereas a section view is illustrated in Figure 6d. This midlithospheric to deep-lithospheric zone of high Vp/Vsh extends under much of the southern and central Gawler Craton; it dips to deeper levels beneath the high-Vsh high-Vp domain to the northeast of Olympic Dam (Figure 6d). As noted above, the position of the gradient (projected to surface) between high- and low-Vp/Vsh domains appears to closely map the distribution of three of the four largest of the IOCG deposits in the Gawler Craton (Prominent Hill, Olympic Dam, and Carrapateena). Interestingly, this gradient extends eastward across the central Curnamona Province, where the few known IOCG deposits (North Portia, Kalkaroo, and Waukaloo) lie within ~50 km of the gradient zone (Figure 5).

4.4. Midlithospheric Discontinuity and Low-Vp/Vsh Layer

Interrogation of the seismic tomographic data has revealed the presence of a relatively low-Vp and low-Vp/Vsh layer in the midlithosphere, with top at ~100 km depth and base at ~130 km depth, and which extends across the northeastern, northern, and central Gawler Craton (Figures 6c and 6d). The possible persistence of the layer beneath the St Peter Suite in the southwest Gawler Craton is unclear (Figure 6d). Although the low-Vp and low-Vp/Vsh layer is not evident in the southern Gawler Craton, mantle-derived garnet xenocrysts carried by Jurassic kimberlites at the Eyre locality of Gaul et al. (2003) record changes in mantle composition

consistent with sharp gradients in coexisting olivine Mg/(Mg + Fe) compositions at depths corresponding to the low-Vp/Vsh layer (~130 km; Figure 6c). The zone of lower Mg/(Mg + Fe) (with values as low as Fo_{88}) at the Eyre locality occurs at a similar depth to that of the low-Vp/Vsh layer to the north. This is consistent with the presence of relicts of the low-Vp/Vsh material at these kimberlite sites, in zones that are perhaps not spatially resolvable in the available seismic tomographic data. Garnet xenocrysts from other kimberlite localities near the southeast margin of the Gawler Craton also exhibit similar compositional gradients, albeit at varying depths (Gaul et al., 2003). A composite section of garnet-based mantle composition for the Gawler Craton shows a major interface at ~130 km depth between an upper, dominantly *fertile*, lithospheric mantle (pale green in garnet-based profile in middle right of Figure 6c) and a lower, dominantly *metasomatized*, lithospheric mantle (dark green and orange in middle right profile in Figure 6c; Gaul et al., 2003). A profile of Vp variation with depth at the Port Augusta kimberlite site (left side of Figure 6c) illustrates the low-Vp zone with minimum velocity of ~8.07 km/s at ~100–110 km depth at this locality. Based on the garnet xenocryst data and imaging of the low-Vp/Vsh layer at similar depths across significant portions of the Gawler Craton, we propose that the base of the low-Vp/Vsh layer corresponds to a midlithospheric discontinuity (MLD) at ~130 km depth. Our results support a previous study identifying an MLD at ~130 km depth beneath the Gawler Craton, based on widely spaced receiver function data (Ford et al., 2010). Similar MLD boundaries have been reported in a number of other cratons with Archean components (e.g., Slave Craton, Snyder, 2008; Snyder et al., 2017; Rader et al., 2015, and references therein). The MLD in the mantle lithosphere of the Gawler Craton is marked mainly by vertical gradients in Vp, without corresponding major changes in Vs, at least at the scales currently resolvable in the AuSREM Vs data. In this regard, the Gawler MLD appears to be somewhat different to the low-Vs MLD zones described by Rader et al. (2015). Higher resolution seismic tomographic data and shear-wave splitting studies will be required to better resolve the nature and depth of the proposed MLD.

4.5. Correlations Between Mafic Geochemistry, Isotope Compositions, and Mantle Domains

Thiel and Heinson (2013) noted the broad spatial relationship between the mantle high-conductivity anomaly C1 and the overlying GRV and Hiltaba Suite. We have built upon this observation by examining the spatial relationships between the geochemical and isotopic compositions of ~1,600–1,575 Ma mafic and alkaline igneous rocks and the electrical conductivity and seismic velocity structure of the underlying lithospheric mantle. Due to the effects of hydrothermal alteration in some parts of the Gawler Craton and Curnamona Province we have utilized trace element discriminants that are generally considered to be relatively immobile during hydrothermal and weathering processes. In particular, the Yb-normalized variations of Th versus Nb (after Pearce, 2008, 2014) have been used to gain insights into possible mantle sources and crustal interactions (Figure 7). An additional screening of the samples for the effects of hydrothermal alteration was also applied, so that samples with exceptionally low or high Na and/or K values, or exceptionally high loss-on-ignition values, were excluded from presentation and interpretation. In Figure 7a the data are presented for basalts and basaltic andesites of the GRV and BVS, as well as for Hiltaba Suite-aged mafic dykes and other intrusive rocks. Also shown for comparison are mafic intrusive rocks of the 1,620–1,610 Ma St Peter Suite. Although some of the coarse-grained mafic intrusive rocks may be cumulates, and hence may not represent liquid compositions, their Th-Nb-Yb compositions are shown for comparison because there appear to be systematic differences in Th-Nb-Yb ratios between intrusive and volcanic rocks spatially across the Gawler Craton and Curnamona Province. A line parallel to the OIB-MORB array demarcating relatively high- versus low-Th/Nb has been positioned to lie immediately below the field of the mafic volcanic rocks (Figure 7a). The available data show that all but one of the localities of basalt and basaltic andesite samples as well as some mafic intrusive rocks have relatively high Th/Nb compositions that are strongly displaced from the MORB-OIB array and plot within the field of continental arcs as defined by Pearce (2008) (Figure 7a). By comparison, and with the important exceptions just noted, most Hiltaba Suite-aged mafic intrusive rocks have higher Nb/Yb and/or lower Th/Yb values than the mafic volcanic rocks, plotting below the line of constant Th/Nb in Figure 7a. Mafic intrusive rocks of the St Peter Suite have continental-arc like Th-Nb-Yb signatures, supporting the conclusion of Swain et al. (2008) of arc-like affinities for the felsic igneous rocks.

Although the data are not yet comprehensive, the spatial distribution of mafic igneous rocks (whether volcanic or intrusive) with high Th/Nb (Figure 7a) shows a rough geographic correlation with the surface-
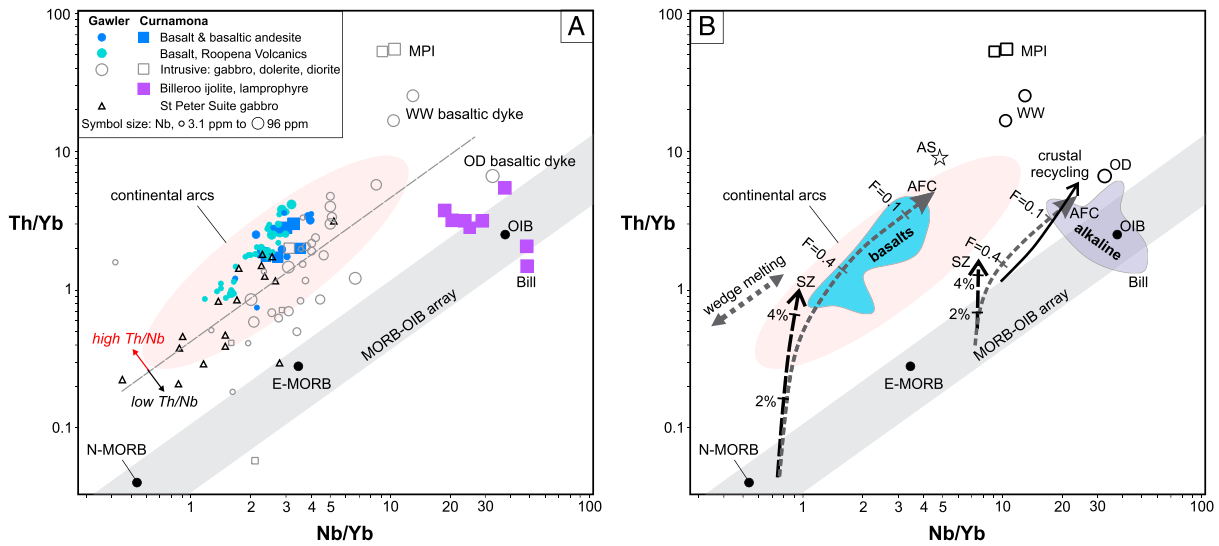
Figure 7. Whole-rock Th-Nb-Yb geochemistry of Gawler Range Volcanics, Benagerie Volcanic Suite, and Hiltaba Suite-aged (~1,595–1,575 Ma) mafic volcanic and mafic to alkaline intrusive rocks from the Gawler Craton and Curnamona Province. (a) Data for mafic volcanic and intrusive rocks, with alkaline intrusive rocks from the Billeroo Complex (Bill) in the southeastern Curnamona Province and mafic intrusives of the ~1,620–1,610 Ma St Peter Suite shown for comparison. Fields for MORB-OIB and continental magmatic arcs from Pearce (2008). A line of constant Th/Nb is shown parallel to the MORB-OIB array; note that most but not all of the ~1,595–1,575 Ma mafic intrusive data points lie below the line (low Th/Nb). Sources of geochemical data: Budd (2006), Wade (2012, and references therein), Wade et al. (2012), Huang et al. (2016), Government of South Australia SARIG database and references therein (data extracted 2017 from https://map.sarig.sa.gov.au), and Geoscience Australia (2007, OZCHEM database and references therein, http://www.ga.gov.au/metadata-gateway/metadata/record/65464/). (b) Field of mafic volcanic data in relation to trajectories of various processes of crust-mantle interaction from Pearce (2008). Abbreviations: AFC, trajectory of assimilation-fractional crystallization for two mantle compositions interacting with Archean crust (see Pearce, 2008 for full description), with fraction of crystallization (F) indicated; AS, average Archean crust; E-MORB, enriched mid ocean ridge basalt; MPI, Mt Painter Inlier mafic intrusion; N-MORB, normal mid-ocean ridge basalt; OD, Olympic Dam; OIB, ocean island basalt; SZ, trajectories of two mantle compositions interacting with a subduction zone component (i.e., subducted sediment-derived; see Pearce, 2008), with percentages of subduction component indicated; WW, Wirrda Well.

projected outline of high-conductivity zones in the sublithospheric mantle in both the Gawler Craton and Curnamona Province (Figure 8; compare red-outlined points and conductivity anomalies). For the Gawler Craton, all of the mafic igneous rocks with high Th/Nb occur above lithospheric mantle with relatively low Vsh seismic wave speed at midlithospheric to deep-lithospheric levels (<4.65 km/s at ~160 km depth; Figure 8). This relationship is supported in the Gawler Craton by the distribution of mafic igneous rocks (both volcanic and intrusive) with relatively low Th/Nb (black-outlined points in Figure 8), which tend to occur more distally from high-conductivity zones and above mantle with relatively high Vsh values. However, the same relationship between mafic geochemistry and Vsh is not apparent in the Curnamona Province. A further limitation is imposed by the sparse distribution of the geochemical samples and by the fact that all of the available data for mafic volcanic units are spatially restricted within and around the high-conductivity anomalies.

Further inferences may be made on the possible origins of the Th-Nb-Yb signatures in Figure 7a by considering several hypothetical trajectories representing modeled mantle-crustal interactions (Figure 7b; Pearce, 2008). These illustrate trends for the processes of (a) modification of mantle with characteristics between those of mid-ocean ridge basalt and ocean island basalt (MORB-OIB array in Figure 6b) by addition of a subduction zone component such as partial melt of subducted sediment (two trends shown in Figure 7b, labeled SZ); (b) assimilation-fractional crystallization of average crust (two trends shown in Figure 7b, labeled assimilation-fractional crystallization, assimilating average Archean crustal component, labeled AS) assuming an r-ratio of 0.3 (see Pearce, 2008); (c) crustal recycling (one trend shown in Figure 7b); and (d) melting of mantle wedge above a subduction zone. As well as showing Th-Nb-Yb compositions typical of continental arcs, the basalts and basaltic andesites exhibit an overall trend subparallel to the MORB-OIB array. This is most clearly evident for the Roopena Basalt, for which 45 analyses are available. Importantly, this trend is subparallel to the mantle wedge melting trend typical of subduction-modified mantle beneath continental arcs. McAvaney and Wade (2015) suggested that the Roopena Basalt was either derived from melting of mantle affected by a previous subduction event or possibly part of a contemporaneous arc-back-arc
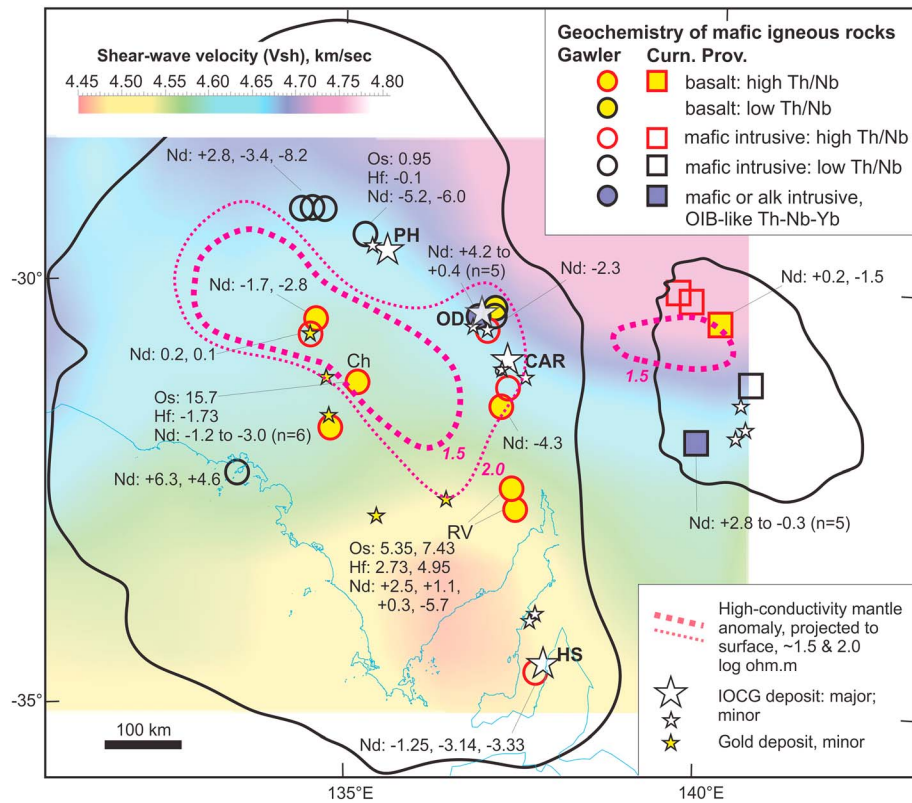
Figure 8. Locations of 1,595–1,575 Ma mafic igneous geochemistry and radiogenic isotope samples, categorized by Th/Yb-Nb/Yb geochemical characteristics from Figure 6a. Background image is S wave velocity (Vsh, depth ~160 km), with outlines of high-conductivity MT anomalies projected to surface from ~80–150 km depth in the Gawler Craton (~1.5 and ~2.0 log ohm-m (~32 and ~100 ohm.m) resistivity contours; Thiel & Heinson, 2013) and from 60 to 110 km in the Curnamona Province (Robertson et al., 2016). Whole-rock epsilon-Nd, epsilon-Hf and ^{187}Os/^{188}Os initial isotope values from Budd (2006), Wade (2012 and references therein), and Pankhurst et al. (2013). Abbreviations: CAR, Carrapateena deposit; Ch, Chitanilga Hill; HS, Hillside; OD, Olympic Dam deposit; PH, Prominent Hill deposit, RV, Roopena Basalt.

system at the time of their generation. Our synthesis supports and extends this interpretation to other mafic volcanics of the GRV and BVS.

The timing of such subduction-related metasomatism is unknown at present. Nevertheless, insights may be gained from the limited available radiogenic isotope data for the mafic igneous rocks (Figure 8). Significantly, two Os isotope analyses for the Roopena Basalt exhibit extremely high ^{187}Os/^{188}Os$_i$ ratios of 5.3 and 7.4 (Pankhurst et al., 2013). These very radiogenic Os isotope compositions could be due to either mixing of a mantle source with a highly evolved crustal contaminant (e.g., 3.1 Ga Archean crust; Pankhurst et al., 2013) and/or due to involvement of high-Re/Os metasomatic agents such as subduction-related fluids (Pankhurst et al., 2013). Given the subduction-modified mantle source interpreted from the Th-Nb-Yb geochemistry (Figure 7a) and the presence of relatively primitive Nd and Hf isotope end-member compositions in some of the Roopena Basalt samples, we favor the latter explanation, that is, significant involvement of a subduction-modified lithospheric component. The highly radiogenic Os isotope signature suggests that this mantle metasomatism probably occurred long before the emplacement of the Roopena Basalt, possibly as early as the Archean. The osmium isotope composition of another GRV sample (basaltic trachy-andesite from *Chitanilga* in the central Gawler Craton; Figure 8) is even more radiogenic (^{187}Os/^{188}Os$_i$ ratio of 15.7; Pankhurst et al., 2013), whereas its $\varepsilon_{Nd(i)}$ values range from −3.0 to −1.2 and it has an $\varepsilon_{Hf(i)}$ composition of −1.7. As for the Roopena Basalt, the Os isotope composition along with continental arc-like Th-Nb-Yb ratios for mafic volcanics at this location (Figures 7a and 8) is consistent with input of a high-Re/Os subduction-related metasomatic component of mantle. However, the evolved Nd and Hf isotope compositions suggest a greater contribution of crustal contaminant than for most Roopena Basalt samples.

A number of samples with high Nb and high Nb/Yb ratios are noteworthy because some are spatially and temporally closely related to IOCG mineralization. The Olympic Dam basaltic dyke sample, while highly altered, is probably representative of one of the key types of ~1,590 Ma mafic intrusive rocks at this deposit (Huang et al., 2016). The two representative Wirrda Well samples reported by Huang et al. (2016) are from much less altered dykes described as olivine-phyric alkali picrite, and which contain igneous apatite with U-Pb an age of ~1,590 Ma. Other, alkaline, mafic intrusive rocks including ijolite (Na-rich) and lamprophyre from the Billeroo Complex in the Curnamona Province (Rutherford et al., 2007), are shown for comparison in Figures 7a and 8, together with two mafic dyke samples with extremely high Th/Yb from the Mt Painter Inlier. Notwithstanding the limited data, it is interesting to note that those samples with high Nb and alkaline-igneous affinities and proximity to known IOCG deposits all occur in the northeastern Gawler Craton or Curnamona Province, within or close to the surface-projected margin of a large high-Vsh mantle domain to the northeast of the Gawler Craton (i.e., between Vsh contours of ~4.62 and ~4.66 km/s; Figure 8).

The mantle sources of the high-Nb mafic and alkaline intrusive rocks appear to have involved an enriched component similar to that of OIB or E-MORB (Figure 7b). The compositions of those rocks with Nb/Yb values up to ~5 (above the MORB-OIB array, including the Olympic Dam and Billeroo samples) could be explained by assimilation of a crustal component into an enriched mantle source (ACF trend; Figure 7b) or by low-degree partial melting of crust that had been recycled into the mantle (Figure 7b; Pearce, 2008, 2014). The extreme compositions of the Wirrda Well and Mt Painter Inlier mafic dykes are more difficult to explain, but Huang et al. (2016) likened the Wirrda Well compositions to those of alkali picrites from the East China Craton that have been interpreted to have formed by a variant of crustal recycling involving lithospheric foundering (Gao et al., 2008).

4.6. Sources of Electrical Conductivity and Seismic Velocity Variations in the Lithospheric Mantle

Characterization of the seismic velocity and electrical conductivity properties of lithospheric mantle domains, and interpreted present-day lithospheric architecture of the Gawler Craton region, are summarized in Figure 6e. We now attempt to explain the origins of this architecture in terms of mantle compositional variations, focusing on the following three key features of the lithospheric architecture:

1. The zone of high electrical conductivity partly within and partly above a broad zone of low seismic (S wave) velocities and high Vp/Vsh in midlevel to deep parts of the lithospheric mantle of the central and southern Gawler Craton (labeled (a) and (b) in Figure 6e).
2. The zone of very high Vp/Vsh within upper mantle largely beneath the St Peter Suite in the southwestern part of the Gawler Craton (labeled (c) in Figure 6e).
3. The low-Vp (and low-Vp/Vsh) layer at midlithospheric depths coincident with compositional changes in lithospheric mantle-derived garnets, which extends into a mantle domain of high Vs to the northeast of Olympic Dam (labeled (d) and (e) in Figure 6e).

4.6.1. Origins of Electrical Conductivity in the Lithospheric Mantle

Interpretation of the sources of enhanced electrical conductivity in the lithospheric mantle is limited by a paucity of experimental data on the conductivity of mantle minerals and their aggregates at appropriately high temperatures and pressures and water contents. Nevertheless, there are sufficient known electrical properties to enable some constraints to be placed on possible sources. These sources may be further constrained by examining correlations with the seismic velocity variations and their possible causes.

Temperature is a key control on mantle conductivity (Jones et al., 2009); however, in the case of the Gawler Craton it is evident that the deep zone of high conductivity (anomaly C1) resides within the present-day lithospheric mantle (based on the lithosphere-asthenosphere boundary [LAB] of Czarnota et al., 2013) or mostly within the lithosphere (based on the LAB of Kennett et al., 2013; Figure 6). The top of the anomaly, as defined by a 10 ohm.m resistivity isosurface, is situated at depths of ~100–150 km (Thiel & Heinson, 2013; see also supporting information, 3-D model); the thickness and depth to the base of the high-conductivity zone (nominally ~200 km) are not well constrained due to the lack of sensitivity for the base of conductive zones in the MT inversion modeling (Thiel & Heinson, 2013). The better constrained upper parts of the high-conductivity zone coincide with the low-Vp/Vsh layer, whereas the central and lower parts of the anomaly are situated within a zone of relatively low Vsh and high Vp/Vsh. Given the location of the high-conductivity zone wholly or mostly within the Precambrian lithospheric mantle local temperature
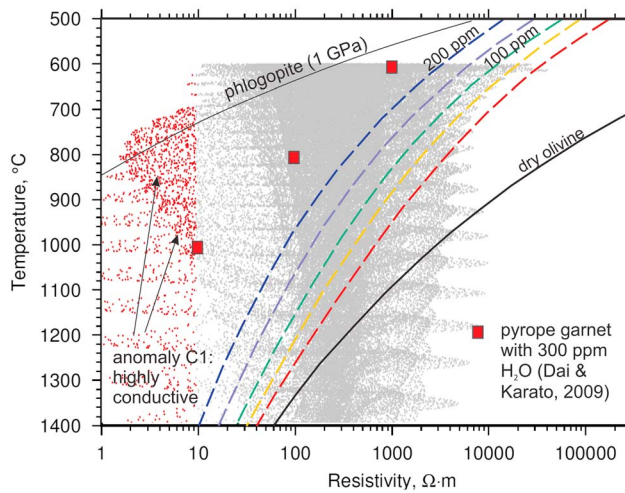
Figure 9. Electrical resistivity values (grey and red points) for cells in the 3-D model of magnetotelluric data of Thiel and Heinson (2013) for the Gawler Craton, presented for temperatures assuming values of 600 °C at the Moho and 1350 °C at the lithosphere-asthenosphere boundary (LAB; Czarnota et al., 2013) and using the geotherm of Tappert et al. (2011). The red points are values of ≲32 ohm.m within the midlithosphere representing the high-conductivity anomaly C1; the grey points represent remaining data from the 3D model. Also shown are curves for the resistivity of dry olivine and olivine with up to 200 ppm H_2O (Jones, 2016, and references therein), experimentally determined values for hydrous pyrope garnet (Dai & Karato, 2009), and F-rich phlogopite (2.3–2.8 wt.% F, curve representing geometrical mean of conductivity of 3 crystallographic directions, Li et al., 2016).

variations seem unlikely to be the principal cause of the elevated conductivity. It is therefore reasonable to deduce that the high conductivities of anomaly C1 are caused by variations in mantle composition. However, the resistivity values as low as 1.3 ohm-m in the model of Thiel and Heinson (2013) represent resistivities up to ~2 orders of magnitude lower than is predicted from the presence of olivine-rich mantle, even if the olivine was water-bearing (Figure 9; see also Pommier & Le-Trong, 2011, and references therein). Other possible candidates among common nominally anhydrous mantle minerals are hydrous garnet, which can attain conductivities up to an order of magnitude higher than water-bearing olivine (Figure 9; Dai & Karato, 2009), clinopyroxene (Yang & McCammon, 2012), graphite, or sulphides (Selway, 2014). Hydrous silicates stable in the mantle such as phlogopite, amphibole or clinohumite (hydrated olivine) also could potentially contribute to elevated electrical conductivity, although there are very few experimental studies. Perhaps of most interest is phlogopite, which may attain very low resistivities (Figure 9), sufficient to yield bulk conductivities of peridotite with 1 vol% phlogopite of up to ~1 ohm.m at 1 GPa and 1200 °C (Li et al., 2016). Although pressure effects were not included in the experiments of Li et al. (2016), the presence of small fractions of phlogopite may at least partly explain the low resistivities of ≲10 ohm.m (Thiel & Heinson, 2013) or ≲1 ohm.m (Thiel et al., 2017) calculated at depths of ~100–150 km (~3–5 GPa) in lithospheric mantle of the Gawler Craton, as proposed by Thiel et al. (2017). High conductivities due to small polaron (i.e., electron) transfer may be possible where an Fe^{2+}/Fe^{3+} couple is present (Selway, 2014). However, the evidence from available whole-rock geochemistry of the mafic GRV (e.g., low V/Ti ratios; Shervais, 1982; Pearce, 2014) suggests that mantle sources of the magmas were not unusually oxidized, and hence, the small polaron mechanism may not be a viable cause in the case of the Gawler Craton mantle electrical anomaly.

4.6.2. Petrological Origins of Seismic Velocity Variations

Further constraints on the properties of the lithospheric mantle can be deduced from comparison of the seismic velocities extracted from published tomographic data with velocities of minerals and rocks calculated using the method of Abers and Hacker (2016) at appropriate temperature and pressure conditions. We utilize the new Vp/Vsh data set for the study area to provide an additional dimension to the interpretation of mantle composition, shown in Figure 10.

In general, for mantle minerals such as olivine and orthopyroxene Vp/Vs increases and Vs decreases as Mg/(Mg + Fe) decreases (see olivine and orthopyroxene curves in Figure 10). Concomitant increases in temperature and pressure along a geotherm also result in increases in Vp/Vs and decreases in Vs for olivine, pyroxene, garnet, and many other mantle minerals (Abers & Hacker, 2016; isotropic velocities), although differences in experimentally determined elastic constants results in significant uncertainties in these trends for some minerals (e.g., see Wagner et al., 2008). Other effects such as anisotropy and anelasticity can also modify Vp/Vs in particular circumstances (e.g., Afonso et al., 2010; Hacker & Abers, 2012). In general terms, lithospheric mantle that is depleted due to the removal of (relatively Fe-rich) partial melts will be characterized by relatively high Vs and low Vp/Vs values. Conversely, mantle that is fertile and relatively Fe-rich generally will exhibit low Vs and high Vp/Vs values; this may also apply where previously depleted mantle has been refertilized and/or metasomatized. A different trend is expected where there is an increase in the orthopyroxene/olivine ratio, resulting in a decrease in both Vp/Vs and Vs, although many other factors (e.g., changes in other mineral abundances and Mg-numbers) will modulate this simplistic trend.

Figure 10 illustrates Vp/Vsh versus Vsh data extracted from the 3-D model for a volume of the Gawler Craton and surrounding regions corresponding to the volume of the 3-D electrical conductivity model of van der Wielen et al. (2016). The general trend of the velocity data extends from low-Vp/Vsh and high-Vsh to high-Vp/Vsh and low-Vsh. In order to better understand the petrological causes of these variations and to link them with other data sets, we examine in detail three end-member scenarios representing some of the
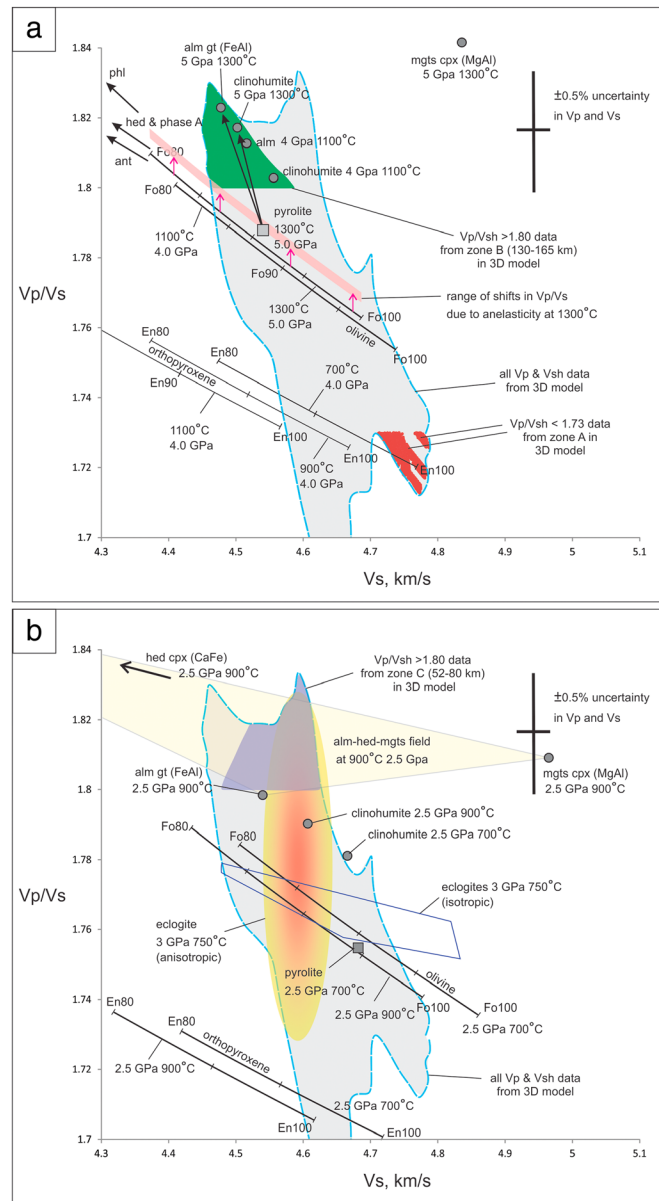
Figure 10. Range of Vp/Vsh versus Vsh data for the Gawler Craton (grey fields), extracted from 3D models (van der Wielen et al., 2016; see supporting information data, 3-D model) of Vsh for the same volume as the 3D model of magnetotelluric data (Thiel & Heinson, 2013), compared to experimentally and theoretically determined Vp/Vs versus Vs velocity characteristics of minerals at two sets of pressure-temperature conditions (calculated using method of Abers & Hacker, 2016). The calculated values are based on isotropic Vs. Each panel shows curves for olivine and orthopyroxene of varying composition (e.g., Fo_{100} to Fo_{80}, En_{100} to En_{80}) at differing pressures and temperatures, constrained by the geotherms of Gaul et al. (2003) and Tappert et al. (2011). (a) For pressures corresponding to depths of 130–165 km depth, the green field represents exceptionally high Vp/Vsh (>1.80) data, and the red field represents exceptionally low Vp/Vsh (<1.73) values. The green field corresponds to zones labeled (a) and (b) in Figure 6e in the central and southern Gawler Craton. Also shown is the effect of anelasticity in olivine (pink band), which becomes significant at >900 °C and causes a shift toward higher Vp/Vsh (Afonso et al., 2010). The red field corresponds to zone (d) in Figure 6e, to the northeast of the Olympic Dam deposit. (b) For pressures corresponding to depths of 52–80 km depth, the purple field outlines exceptionally high Vp/Vsh (low-Vsh) data from zone (c) in Figure 6e, in the southwestern part of the Gawler Craton, compared to mineral data calculated at 2.5 GPa and 900 and 700 °C. Also shown are a hypothetical field for almandine-hedenbergite-tschermakitic clinopyroxene, a field for natural eclogites calculated at 3 GPa 750 °C and assuming isotropic velocities (Worthington et al., 2013), and a field of calculated velocities for one of the eclogite samples assuming anisotropic velocities (shaded yellow and orange field encompasses >60% of possible velocities, Worthington et al., 2013). Abbreviations: alm, almandine (FeAl) garnet; ant, antiorite; gr, grossular (CaAl) garnet; hed, hedenburgite (CaFe) clinopyroxene; jd, jadeite (NaAl) clinopyroxene; mgts, MgAl tschermakitic clinopyroxene; phl, phlogopite.

extremes in the data set (Figures 10a and 10b). We focus on these end-members because there are fewer possible explanations for these extremes than for the bulk of the data, which have large numbers of possible combinations of minerals, and also because the three selected end-members represent the three key parts of the lithospheric architecture enumerated earlier in this section (Figure 6e, labeled (a), (b), and (c) plus (d)). Also shown in Figures 10a and 10b are the velocity characteristics of olivine (Fo_{100} to Fo_{80}) and orthopyroxene (En_{100} to En_{80}) calculated at pressure-temperature conditions appropriate for the depths of each scenario (Abers & Hacker, 2016). To estimate the temperature-pressure conditions in Figure 10, we have utilized two alternative geotherms: a relatively low-temperature geotherm based on garnet xenocrysts from Permian-Jurassic kimberlites intruding the southeastern margin of the Gawler Craton and Neoproterozoic Adelaide Rift Complex (Gaul et al., 2003), and a higher-temperature geotherm based on garnet xenocrysts and garnet- and pyroxene-bearing mantle xenoliths in Jurassic kimberlites from the Monk Hill locality, also in the Adelaide Rift Complex (Tappert et al., 2011). These geotherms bracket the corresponding surface heat flow between approximately 42 mW/m^2 and ~50–60 mW/m^2 (Tappert et al., 2011).

4.6.3. Mid-level to Deep Lithospheric Zone of Low Velocity and High Conductivity

Figure 10a illustrates data from a mid-level to deep lithospheric zone (below ~130 km) in the central and southern Gawler Craton characterized by very high Vp/Vsh, low Vsh, and low Vsv (green field with Vp/Vsh > 1.80 in Figure 10a). This zone (labeled (b) in Figure 6e) is important because it spatially overlaps with the zone of anomalously high electrical conductivity (labeled (a) in Figure 6e), and its northeastern boundary lies directly beneath the northwest-southeast trend of major IOCG deposits (Olympic Dam, Prominent Hill, and Carrapateena; Figures 5a and 5c). At conditions of 4 GPa 1100 °C to 5 GPa 1300 °C (based on geotherms of Gaul et al., 2003, and Tappert et al., 2011) the data with Vp/Vsh > 1.80 lie significantly above the curves for olivine, even taking into account the effects of anelasticity, which results in increases in Vp/Vs ratios of olivine at temperatures above 900 °C (Figure 10a; Afonso et al., 2010). Few minerals stable at these mantle conditions would result in Vp/Vs ratios above those of olivine at a given Vs value; almandine (FeAl) garnet and MgAl-tschermak-rich clinopyroxene are two such minerals, whereas addition of phlogopite, serpentine (antigorite), or hedenbergite (CaAl clinopyroxene) would not yield trends toward the extreme high Vp/Vsh velocities observed in the model (Figure 10a). However, the conversion of olivine to the hydrated form, clinohumite, with or without almandine, could account for the calculated velocity properties of the deep high-Vp/Vsh and low-Vsh zone (based on Abers & Hacker, 2016). No electrical conductivity data are available for clinohumite. Nevertheless, it is possible that the presence of this OH-bearing phase along with water-rich olivine potentially also could contribute to the high electrical conductivity of zone (a) in Figure 6e that occurs partly within the high-Vp/Vsh low-Vsh zone. Although the addition of phlogopite to peridotite could also account for the observed high conductivity in this zone, noted above (Thiel et al., 2017), it is unlikely to account for the decrease in Vsh and increase in Vp/Vsh observed in zones (a) and (b) in Figure 6e. This is because the (negative) slope of phlogopite addition to peridotite in Figure 10a seems inconsistent with the observed high-Vp/Vsh data, and moreover, much of the high-Vp/Vsh zone (b) is much less conductive than zone (a).

4.6.4. High-Vp/Vsh Zone Northeast of Olympic Dam

A second set of data (Figure 10a, red field) represents a zone of extremely low Vp/Vsh and high Vsh (and high Vsv) at depths of ~100–150 km to the northeast of the Olympic Dam deposit. These data correspond to the zone labeled (d) in Figure 6e. Data with Vp/Vsh < 1.73 from this zone lie beyond the limit of olivine-orthopyroxene-rich highly depleted mantle rocks (e.g., with olivine Mg-number > Fo_{93} and orthopyroxene Mg-number > En_{93}). However, velocities of end-member enstatite at 4 GPa and a very cool geotherm condition of 700 °C are consistent with the observed data (Figure 10b). Unusually low Vp/Vs ratios have been explained elsewhere (e.g., in subduction zone mantle wedges) as the result of enstatite-rich mantle (Wagner et al., 2008) or quartz-rich mantle (Rossi et al., 2006). However, these origins were questioned by Hacker and Abers (2012), who suggested that such low Vp/Vs values could result from anisotropy within *normal* peridotite. Available data do not allow us to discriminate between these possible origins. Nevertheless, it is apparent from the Vp data in Figure 6c and Vp/Vsh image in Figure 6d that the midlithospheric zone of low Vp/Vsh not only is present in the high-Vsh (and high-Vsv) domain to the northeast of Olympic Dam but also occurs throughout the central and southern Gawler Craton (labeled (e) in Figure 6e; see also supporting information, 3-D model). In this latter region, where the same low-Vp layer has less extreme values of Vp/Vsh than to the northeast of Oympic Dam, Gaul et al. (2003) reported the minor presence of

harzburgitic (i.e., olivine-orthopyroxene peridotite) garnets in kimberlites. These garnets were sourced from depths of ~100–170 km, which overlaps in depth with the low-Vp and low Vp/Vsh layer at ~100–130 km depth, and suggests that relicts of harzburgite may be present at the depths of the low-Vp layer. For this reason, we infer that the unusually low Vp/Vsh midlithospheric layer is orthopyroxene-rich to the northeast of Olympic Dam and transitions laterally into a less orthopyroxene-rich yet overall pyroxenitic composition in the central and southern Gawler Craton.

4.6.5. High-Vp/Vsh Zone Beneath St Peter Suite

The third scenario (Figure 10b) represents shallow lithospheric mantle conditions (~50–80 km depth) where a zone of extremely high Vp/Vsh (>1.80) occurs in the southwestern part of the Gawler Craton largely beneath the St Peter Suite (Figures 5d and 6d; labeled zone (c) in Figure 6e). At these conditions the anomalously high-Vp/Vsh data lie well above the Vp/Vs velocity properties of olivine, and are difficult to explain by the presence of any common mantle minerals, if isotropy of seismic velocities of minerals is assumed (as in the calculation method of Abers & Hacker, 2016). Addition of clinohumite increases Vp/Vs insufficiently and high Vp/Vs minerals such as cordierite or spinel would be either not stable or present in such minor quantities as to not significantly displace velocities above those of olivine. Combinations of hedenbergite, almandine, and/or MgAl-rich tschermakitic clinopyroxene conceivably could account for the observed velocities, but these end-members are not normally abundant in lithospheric mantle (e.g., Slave Craton; Kopylova et al., 2004). Serpentinization of uppermost mantle has been suggested to explain very high Vp/Vs values in some mantle wedges above subducting slabs (e.g., Rossi et al., 2006), but addition of antigorite would result in lower Vs values than those for the observed Vp/Vsh values >1.80 (Abers & Hacker, 2016). Moreover, the shallow-mantle zone with high Vp/Vsh is relatively resistive in the model of Thiel and Heinson (2013), which may be inconsistent with the presence of significant amounts of hydrated minerals. Crustal rocks, particularly those of mafic composition such as gabbro, may have high Vp/Vs values (e.g., Behn & Kelemen, 2006), but these too have Vs values below the observed values. Eclogites can have high Vp/Vs and Vs values relative to peridotites and may attain Vp/Vs values of up to ~1.80 at 2.5–3.0 GPa 700–900 °C (Figure 10b; Kopylova et al., 2004; Worthington et al., 2013). When the effects of anisotropy are also considered for eclogites, even higher Vp/Vs values may be explained (Figure 10b; Worthington et al., 2013). In summary, we favor eclogite with an Fe-rich bulk composition relative to depleted peridotite, with or without anisotropic structure (e.g., foliated), as the most likely source of the shallow-mantle high-Vp/Vsh zone. This zone could be considered an *underplate* of mafic (basaltic/gabbroic) igneous origin, as recognized in a range of geological environments (Thybo & Artemieva, 2013).
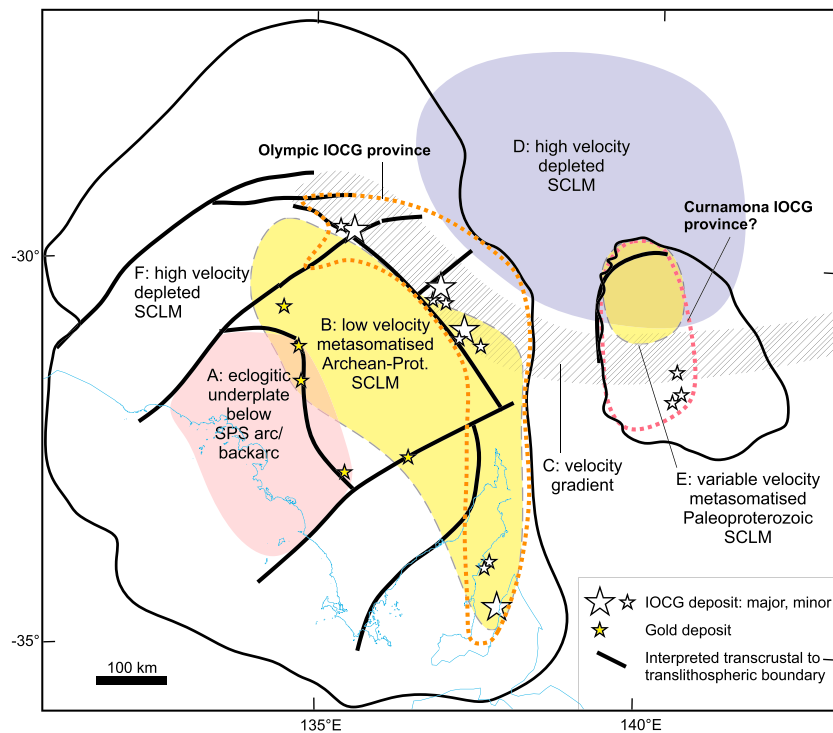
4.7. Summary of Lithospheric Mantle Domains

Figure 11 illustrates the interpreted mantle lithospheric architecture in the Gawler Craton and Curnamona Province in relation to known Early Mesoproterozoic IOCG and gold deposits. The boundaries of the domains (labeled A–F) are not sharply defined but are inferred from the synthesis of the seismic tomographic, MT, whole-rock geochemical and isotopic, geological, geochronological, and mantle xenocryst data sets. The architecture of transcrustal to translithospheric faults/boundary zones is derived from previous geological mapping (Cowley, 2008) and from the interpretation of Skirrow (2010).

Overall, the observed present-day lithospheric architecture is interpreted to image the transition from a Paleoproterozoic arc or back-arc (domain A, Figure 11) across the margin of an Archean-Mesoproterozoic continental fragment with metasomatized lithospheric mantle (domain B), and thence northeastward and northward into domains of highly depleted lithosphere (D and F). The major IOCG deposits occur along the inboard margin of metasomatized mantle, whereas the gold deposits are localized nearer the transition from the relatively primitive arc or back-arc domain A and the older more evolved continental fragment.

5. Discussion

In the foregoing we have placed constraints on possible mineralogical compositions of key domains within the lithospheric mantle of the Gawler Craton and Curnamona Province, by consideration of seismic velocity and electrical conductivity data, theoretical and experimental data on rock properties, and garnet xenocryst data from kimberlites. A key aim of the study, and the focus of the discussion below, is to explain the observed architecture in terms of the tectonic and geological evolution of the Gawler Craton and Curnamona Province and their IOCG mineral systems. First, previous models of the tectonic settings and

Figure 11. Interpreted lithospheric mantle domains in the Gawler Craton and Curnamona Province (this study), in relation to inferred trans-crustal to trans-lithospheric fault/shear/boundary zones (based on Skirrow, 2010).

geodynamic processes are briefly reviewed, and an alternative model is introduced. We then discuss the key stages of the evolution, integrating the lithospheric architecture with constraints from known geology, geochronology and igneous geochemistry. Finally, we present some inferences on possible relationships between IOCG ore formation, lithospheric architecture, and mantle metasomatism. The proposed model is a working hypothesis that can be tested with new data and observations.

5.1. Previous Tectonic Models and Lithospheric Foundering

Previous models of an *anorogenic* tectonic setting of the Gawler Craton and Curnamona Province during emplacement of the Hiltaba Suite, GRV and major IOCG deposits, involving mantle upwellings/plumes or hot spots (e.g., Giles, 1988; Groves et al., 2010; Hitzman, 2000), are inconsistent with the syn-deformational, synorogenic, emplacement of the early phases of the Hiltaba Suite and the early IOCG-related regional Na ± Ca and Fe-K alteration (Hand et al., 2007; Hayward & Skirrow, 2010; Skirrow et al., 2002; Skirrow et al., 2007). The Hiltaba Suite and GRV have been described as constituting part of a silicic or felsic large igneous province (Allen et al., 2008), underlining the observation that exposed remnants of this magmatic event are felsic-dominated. This is unlike the igneous products of most plume- or hot spot-related magmatism, which are generally asthenosphere-derived and tholeiitic basalt-dominated (Ernst, 2014). Indeed, our interpretation of available geochemistry for the mafic components of the GRV and BVS supports and extends that of McAvaney and Wade (2015), who suggested that there was a significant subduction-modified lithospheric component within the mantle source region of the Roopena Basalt. While this lithospheric component conceivably could have been part of an ascending mantle plume (e.g., recycled crust), the geochemical signature equally can be explained by partial melting of metasomatized lithospheric mantle. Moreover, the temperature of the source region of GRV basalts (~1380 °C at 50–60 km depth; Foden et al., 2016) is not as high as might be expected for a plume source (Ernst, 2014).

Supra-subduction zone settings have been proposed for some IOCG deposits, particularly those in Andean environments in Chile and Peru (e.g., Hitzman, 2000; Sillitoe, 2003; Groves et al., 2010; Richards & Mumin, 2013). A Paleoproterozoic Andean-type environment was proposed by Ootes et al. (2017) for IOCG and iron oxide-apatite deposits in the Great Bear Magmatic Zone in Canada. The setting is characterized by high-K

calc-alkaline and shoshonitic igneous rocks of mostly intermediate to felsic composition, which were mostly emplaced following a tectonic switching from compression to extension. The extension-related magmatism was interpreted by Ootes et al. (2017) to have resulted from stalling of the Great Bear slab after subduction reinitiation further outboard of the continental margin.

Although the lithospheric architecture described for the Gawler Craton in this study images what we interpret to be a late Paleoproterozoic arc or back-arc at a continental margin (the St Peter Suite), a suprasubduction setting at the time of IOCG deposit formation at ~1,595–1,575 Ma does not fully account for several of the key observed geological features. In particular, the A-type compositions of major parts of the Hiltaba Suite and GRV silicic large igneous province (Allen et al., 2008) are atypical of subduction-related magmatism within magmatic arcs (Budd, 2006). Nor is the subcircular (equant) spatial distribution of this felsic magmatism very similar to the typically linear belts of magmatic arcs, although it could be argued that the current distribution does not represent the original arc geometry. Finally, wholesale and major stretching of the lithosphere (e.g., beta-factor > 2), as may occur within a well developed continental back-arc basin or intracontinental rift setting, is likely to result in basins of substantial (multikilometre) thickness. Such basins are not observed in the Gawler Craton and Curnamona Province for the period 1,610–1,575 Ma, although relatively thin (<1–2 km?) sedimentary sequences were deposited in places during this period (e.g., Corunna Conglomerate, sediments intercalated with the Roopena Basalt and with the GRV at the Olympic Dam deposit; Curtis et al., 2018; McAvaney & Wade, 2015; McPhie et al., 2011, 2016).

Betts et al. (2009) accounted for the Olarian Orogeny and the temporally and spatially overlapping Hiltaba Suite and GRV in a model combining a hot spot (beneath an oceanic plateau) and subduction at a continental margin. They contended that migration of the cratonic lithosphere relative to the hot spot resulted in a shift of hot spot-related magmatism into the Mt Isa region; associated A-type granitic magmatism is spatially and temporally related to the ~1,530–1,500 Ma IOCG ore-forming systems in the Cloncurry district (Figure 2; Duncan et al., 2011). However, we argued above that the evidence for a mantle plume or hot spot-related origin of the GRV and Hiltaba Suite is not strong, and the model of the hot spot ascending across or around the subducting slab (e.g., at tears/discontinuities, Betts et al., 2012) requires coincidental geodynamic processes that are probably unnecessary to account for the observed lithospheric architecture and evolution of the Gawler Craton and Curnamona Province.

Given the shortcomings of previously proposed settings, an alternative geodynamic and tectonic model is required that is consistent with the observed lithospheric architecture described herein, geological event history and igneous geochemistry. We propose that thinning of the lithospheric mantle by foundering, or delamination, rather than by wholesale stretching, best explains the observations. This concept builds on previous suggestions of lithospheric delamination that were mentioned as one of several possible drivers for particular igneous suites in the region (Ferris et al., 2002; Rutherford, 2006), and further develops the Gawler-Curnamona-wide model of lithospheric removal presented by Skirrow (2010, 2016).

Lithospheric foundering (including both the *delamination* and Rayleigh-Taylor convective removal processes; e.g., Bird, 1979; Houseman & Molnar, 2001; Houseman et al., 1981; Kay & Kay, 1993; Schott & Schmeling, 1998) has been proposed for many terranes and settings globally, and active delamination has been geophysically imaged in some modern settings (e.g., Andes, Schurr et al., 2006; Beck et al., 2015, Murray et al., 2015; Tibetan Plateau, Chen et al., 2017; western Mediterranean region, Fadil et al., 2006; east Carpathians, Chalot-Prat & Girbacea, 2000; Colorado Plateau, Levander et al., 2011; New Zealand, Hoernle et al., 2006; and Africa, Hu et al., 2018). Although Archean lithospheric mantle is widely considered to have remained relatively immune from destruction due to its commonly melt-depleted composition and hence buoyancy and strong rheology (e.g., Djomani et al., 2001), thinning by removal of parts of Archean subcontinental lithospheric mantle has been well demonstrated for several cratons. These include the eastern part of the North China Craton (Gao et al., 2008) and the western part of the Wyoming Craton (Snyder et al., 2017, and references therein). The mechanisms of lithosphere removal in these regions are the subject of continuing debate. Nevertheless, our review of lithospheric foundering including numerical modeling studies (e.g., Babeyko et al., 2002; Gorczyk & Vogt, 2015; Krystopowicz & Currie, 2013; Morency et al., 2002) indicates that there are several major geological consequences of lithospheric foundering. The observables include (1) evidence of rapid uplift (up to 1–4 km over time scales of a few million to tens of millions of years) preceded and/or flanked by relatively small and thin (<1–2 km) basins, (2) volcanics deposited on the unconformity caused by the uplift and

exhumation, (3) potassic to ultrapotassic mafic/ultramafic magmatism (in places hydrous) derived from partial melting of lithospheric mantle, (4) *adakitic* magmatism, (5) high-temperature crustal melting, (6) bimodal magmatism, (7) high-temperature low-pressure metamorphism, and (8) a switch from compression to extension over time periods of a few million to tens of millions of years. Although each observable may result from processes other than lithospheric removal, the combination of several or all of these geological consequences will more strongly support a hypothesis of lithospheric foundering in a given region. We postulate that most of these geological characteristics are present in the Gawler Craton and Curnamona Province, and we therefore conclude that lithospheric foundering is the best explanation for the driver of mantle melting and thence crustal melting during the period ~1,595–1,575 Ma. Evidence supporting a model of lithospheric foundering is discussed further below.

5.2. Preferred Geodynamic Model and Tectonic Setting of IOCG Hydrothermal Systems

Although there remain many uncertainties in the characterization of the lithospheric architecture, mantle compositions, and timing of events, we believe that sufficient data are now available to propose a new working hypothesis of the geodynamic and tectonic evolution of the Gawler Craton and Curnamona Province and the IOCG ore-forming systems. In brief, the proposed model involves the following events: (i) Archean-Paleoproterozoic construction of two layers of lithospheric mantle separated by an MLD; (ii) late Paleoproterozoic subduction-related magmatism accompanied by metasomatism and refertilization of sub-Gawler and sub-Curnamona lithospheric mantle; (iii) orogenesis associated with accretion of a *collider*, which triggered gravitational destabilization of metasomatized and refertilized lithospheric mantle; (iv) late Paleoproterozoic to early Mesoproterozoic foundering of previously refertilized and/or metasomatized lithospheric mantle, accompanied by a switch from compression to extension and widespread mafic and A-type felsic magmatism; and (v) IOCG mineral system formation at ~1,595–1,575 Ma above zones of lithospheric thinning, driven by heat from mafic and felsic magmatism, and controlled spatially by trans-lithospheric breaks between lithospheric blocks.

These events are discussed below and are illustrated in Figure 12.

5.2.1. Archean-Paleoproterozoic Lithospheric Growth and MLD Development (3,150–1,700 Ma)

Highly depleted lithospheric mantle, typical of the residue resulting from komatiitic melt extraction (e.g., Arndt et al., 2009), is inferred to have formed during the period from >3,150 to ~2,500 Ma (Figure 12, top panel). The base of this ~130-km-thick layer is traversed by an ~30- to 50-km thick layer with low Vp and low Vp/Vsh, inferred to be variably orthopyroxene-rich (Figures 6c–6e). We place the timing of this orthopyroxene-producing metasomatism as prior to the stacking or subcretion of a second, underlying, lithospheric layer because it is difficult to envisage how such an extensive layer of low-Vp mantle could have developed internally within depleted lithospheric mantle that was already thicker than ~120–130 km. Although Eeken et al. (2018) described the intralithospheric development of low-velocity zones at MLDs above ~100–150 km depth in several Archean and Proterozoic cratons it is not clear whether such metasomatic processes could have produced the laterally extensive MLD inferred in the lithosphere of the Gawler Craton. Accordingly, in our model during the period ~2,500–1,700 Ma (Figure 12), we infer that a second lithospheric layer was stacked beneath, or subcreted to, the upper lithospheric layer, in order to explain the presence of a lower layer of lithosphere (below ~125 km depth) with highly depleted composition (inferred from very high Vs values to the northeast of Olympic Dam, and mantle-derived garnet xenocryst compositions, Gaul et al., 2003). Based on the models described by Snyder (2008) and Snyder et al. (2017) for the Slave craton and other Archean-Proterozoic cratons, we envisage the two-layered Gawler-Curnamona lithospheric mantle to have formed by under-thrusting and stacking of lithospheric layers or by subcretion of mantle plume residues. Neodymium isotope data for felsic igneous rocks also support the proposal of lithospheric growth during the period 2,500–1,700 Ma rocks (Figure 5d, shades of yellow and green).

5.2.2. Paleoproterozoic Subduction-Related Magmatism and Mantle Metasomatism (1,700–1,610 Ma)

We argued earlier that the low Vsh and high Vp/Vsh values at depths beneath ~130 km (labeled zone (b) in Figure 6e and domain B in Figure 11) are most likely due to relatively Fe-rich fertile peridotite that may contain minerals such as clinohumite and/or particular pyroxene and/or garnet types with unusually high Vp/Vs characteristics. This is supported by evidence, from mantle-derived garnets, for the presence of metasomatized and/or refertilized mantle that extends to depths of almost 200 km in the southern Gawler Craton and its southeastern margins (Gaul et al., 2003; Tappert et al., 2011). However, the garnet xenocryst data
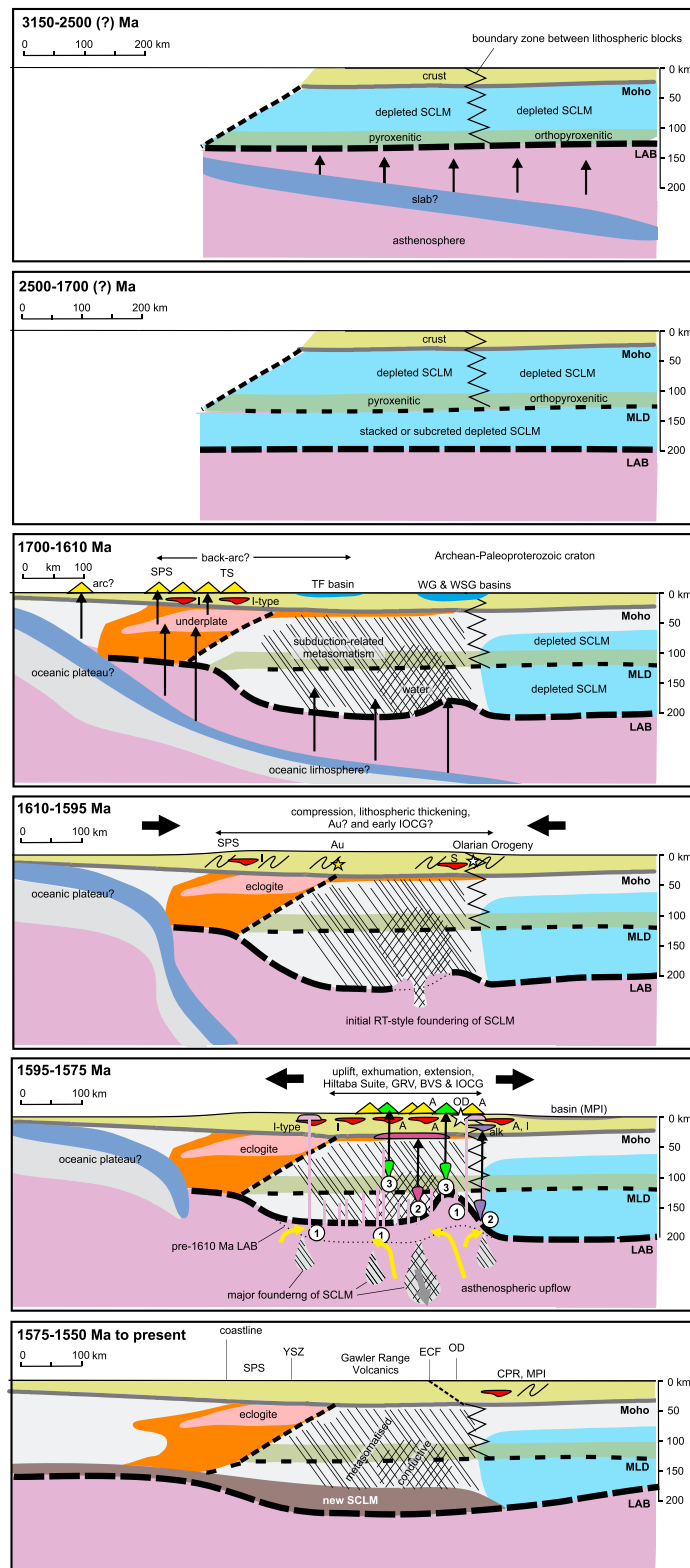
Figure 12. Interpreted evolution of the Gawler Craton and Curnamona Province, cross-sectional view, southwest to left, northeast to right (schematically the XS-XS′ line in Figure 1). See text for details. Abbreviations: LAB, lithosphere-asthenosphere boundary; SPS, St Peter Suite; TS, Tunkillia Suite; MLD, midlithospheric discontinuity; SCLM, subcontinental lithospheric mantle; TF, Tarcoola Formation; YSZ, Yarlbrinda Shear Zone; ECF, Elizabeth Creek Fault; OD, Olympic Dam deposit; CPR, Coober Pedy Ridge; MPI, Mt Painter Inlier.

also indicate the preservation of highly depleted lithospheric mantle in the same regions sampled by the Permian and Jurassic kimberlites (Gaul et al., 2003; Tappert et al., 2011).

These observations are most simply reconciled in a model whereby the two-layered depleted Archean-Paleoproterozoic lithospheric mantle was overprinted selectively in the central and southern Gawler Craton and southern Curnamona Province by locally intense mantle-derived metasomatism and refertilization. The timing of such processes is unclear, and indeed, multiple events from the Archean to the Mesozoic breakup of Gondwana may have produced the observed seismic velocity (and electrical conductivity) variations. Nevertheless, our working hypothesis is that this metasomatism and refertilization was related to east-dipping subduction represented by the magmatism of the Tunkillia Suite and the St Peter Suite during the period ~1,700–1,610 Ma (Figures 2 and 12; Ferris et al., 2002; cf. Swain et al., 2008). This conclusion is drawn from (i) the observation that these igneous suites are distributed partly above and to the west-southwest of the region of mid-level to deep lithospheric refertilization and metasomatism (Figure 1; zone (b) in Figure 6e; domain A in Figure 11) and (ii) that subduction-related processes are an obvious means of introducing water-bearing metasomatic fluids/melts into the lithospheric mantle. Mantle plume-related processes (e.g., ~830 Ma Gairdner LIP) and rifting during continental breakup in the Mesozoic seem less favorable mechanisms of introducing water-bearing fluids/melts within the central part of the Gawler Craton.

The results of the present study support the presence of a preserved mafic underplate beneath the St Peter Suite (sections 4.3 and 4.6.5). The unusually high Vp/Vsh characteristics of the lithospheric mantle directly beneath the St Peter Suite at ~40–70 km depth are consistent with the presence of an eclogitic (as opposed to peridotitic) body. Such material may be expected where basaltic/gabbroic material was emplaced at, and/or below, the Moho beneath a magmatic arc or back-arc, and thence converted to eclogite either at the ambient pressure-temperature conditions of emplacement (e.g., Behn & Kelemen, 2006), or during thickening of the underplate caused by compressional orogenesis (e.g., Krystopowicz & Currie, 2013). Our results therefore support a model of east or northeast dipping (in present coordinates) subduction beneath the St Peter Suite, as suggested by Betts et al. (2009). Compressional deformation during and/or shortly after emplacement of the St Peter Suite (Hand et al., 2007) conceivably provided a mechanism for eclogite derivation from a mafic underplate. As shown in Figure 12 (1,700–1,610 Ma panel) a possible driver of lithospheric shortening was the collision/accretion of a buoyant collider such as an oceanic plateau (Betts et al., 2009), although we suggest that an active *hot spot* beneath the oceanic plateau was not necessarily present. This direction of dip of the subduction zone places the St Peter Suite at the continental margin of the Gawler Craton, in a possible back-arc position.

5.2.3. Lithospheric Foundering, Magmatism, and IOCG Formation (1,610–1,575 Ma)

The period 1,610–1,595 Ma is envisaged to have involved the accretion or subduction of a collider of oceanic plateau or island arc at the southwestern margin (outboard of the St Peter Suite, not observed/preserved), which resulted in a major orogenic event. The deformation and metamorphism is recognized in the Curnamona Province as the Olarian Orogeny (Figure 2; Betts et al., 2009) and also affected parts of the Gawler Craton where it was partitioned into major trans-crustal to trans-lithospheric weaknesses such as the Kalinjala Shear Zone (Betts et al., 2009; Reid & Hand, 2012). We propose that lithospheric mantle was gravitationally destabilized during the orogenic event, related to compressional thickening of the lithosphere. This is consistent with a number of studies showing that gravitational instabilities may be initiated during compressional thickening of previously refertilized, metasomatized, and weakened lithospheric mantle, and at steps in the depth of the LAB (e.g., Bao et al., 2014; Gorczyk & Vogt, 2015; Krystopowicz & Currie, 2013; Levander et al., 2011; Li et al., 2008; van Wijk et al., 2010). The combination of metasomatized mantle and gradients in the LAB may have existed beneath the Wallaroo Group basin along the eastern margin of the Gawler Craton and in the central-southern Curnamona Province beneath the Willyama Supergroup (Figure 2). We therefore suggest that foundering, or delamination, may have initiated in these areas.

After ~1,595 Ma, Rayleigh-Taylor type *dripping* of gravitationally unstable and weak lowermost lithosphere is envisaged to have expanded and migrated westward and southward from the areas of initial foundering. This interpretation of migration is based on the timing of Hiltaba Suite magmatism, which shows a general westward and southwestward younging as well as a change from dominantly A-type in the eastern and central Gawler Craton to dominantly high-temperature I-type in the western part of the craton (Figure 1; Budd, 2006). This felsic-dominated magmatism, along with the GRV and BVS, are considered to be the crustal melting manifestation of mantle melting and heat transfer (Budd, 2006; Creaser, 1996; Giles, 1988; Stewart, 1994).

The likely presence of hydrous-metasomatized lithospheric mantle in the central Gawler Craton (Thiel & Heinson, 2013; this study) provides both a locus for continued foundering of Precambrian lithospheric mantle and for partial melting of lithospheric mantle. The speculated migration in foundering could have resulted in almost complete removal of the lower part of lithospheric mantle beneath the central and southern Gawler Craton and southern Curnamona Province, explaining the equant *footprint* of Hiltaba Suite and GRV magmatism beneath the central part of the Gawler Craton. Lithospheric foundering also is consistent with evidence for uplift and exhumation in the Olympic Dam region between the emplacement of the host granite at ~1,595 Ma at depths of 5–6 km (Creaser, 1996) and the formation of the ore deposit in a near-surface environment at ~1,590 Ma together with emplacement of the GRV (Johnson & Cross, 1995; Reeve et al., 1990). Over a similar time period, we infer uplift and exhumation in the western Curnamona Province, where rocks metamorphosed in the upper greenschist facies during the Olarian Orogeny at ~1,600 Ma are overlain by essentially unmetamorphosed and flat-lying volcanics of the BVS at ~1,587 Ma (Wade et al., 2012). These observations imply multikilometer uplift and exhumation between ~1,600 and 1,587 Ma.

Theoretical considerations and numerical modeling of lithospheric removal processes (e.g., Gorczyk & Vogt, 2015; Lustrino, 2005) demonstrate that replacement of the space occupied by foundered lithosphere by asthenosphere can result in decompressional melting of the ascending asthenospheric mantle as well as heating by conduction and melting of previously metasomatized and/or refertilized zones within lithospheric mantle newly exposed to convecting mantle. Mantle depleted of partial melts during this process is represented by the relatively high-Vs lowermost layer of lithospheric mantle in the Gawler Craton, beneath zones (a) and (b) in Figure 6e and labeled *new SCLM* in Figure 12 (1,575–1,550 Ma panel).

Sources of partial melts generated by adiabatic decompression of ascending asthenospheric mantle are labeled (1) in Figure 12 (1,595–1,575 Ma panel). Igneous rocks representing ~1,595–1,575 Ma asthenospheric melts have not been widely identified in the Gawler Craton. Nevertheless, (altered) ultramafic dykes at the Olympic Dam deposit with εNd_{1590} values of approximately +4 (Johnson & McCulloch, 1995) and Th-Nb-Yb ratios near those of OIB (Figure 7a), and gabbros intruding the St Peter Suite with εNd_{1590} values of approximately +6 (Wade, 2012) and Th-Nb-Yb ratios approaching those of E-MORB (Figure 7a) are possible candidates. Contributions from sources with N-MORB- to E-MORB-like trace element geochemical characteristics are also likely for many of the other mafic intrusive rocks of Hiltaba Suite age (Figure 7a), and Stewart (1994) suggested that the parental magmas of the mafic GRV were derived from mixtures of MORB- or OIB-like sources and an enriched (REE- and large-ion lithophile element-rich, ancient subduction-modified) lithospheric source. It was noted earlier, however, that some of the coarse-grained mafic rocks may not represent liquid compositions, and several key units remain to be adequately dated.

Partial melting of previously metasomatized and refertilized lithospheric mantle is envisaged to have occurred at multiple depths (labeled (2) and (3) in Figure 12, 1,595–1,575 Ma panel). Conductive heating of lower lithospheric mantle caused by fresh exposure to convecting mantle conceivably drove partial melting (source (2)). Where the degree of partial melting was low, highly alkaline intrusive rocks were produced such as the lamprophyres, ijolites, and syenites of the Billeroo Complex, which were described by Rutherford et al. (2007) as sourced from subduction-modified lithospheric mantle.

The layer of interpreted pyroxenite-rich mantle above the MLD, where overprinted by subduction-related hydrous metasomatism and refertilization in the central Gawler Craton, was a possible source of partial melting for the mafic GRV (source (3) in Figure 12, 1,595–1,575 Ma panel). This modified ancient (Archean?) source could account for the subduction-related arc-like trace element signatures of the mafic GRV rocks (Huang et al., 2016; this study), the highly radiogenic $^{187}Os/^{188}Os$ values (Pankhurst et al., 2013), and the fertile garnet pyroxenitic composition of the source as modeled by Foden et al. (2016). However, source (3) is deeper than the ~40–50 km proposed by Foden et al. (2016) or the <60 km proposed by Giles (1988); melting columns extending from source (3) to depths as shallow as ~40–60 km may account for this apparent discrepancy (e.g., Havlin et al., 2013; Plank & Forsyth, 2016). Heating at the level of hypothetical source (3) may have been caused by conduction from asthenospheric as well as deep-lithosphere derived melts, sufficient to drive moderate- to high-degree partial melting of the partially hydrous and fertile midlithospheric source. Alternative, deeper, sources of the mafic GRV (e.g., fertile material entrained within a mantle plume) would require even longer melting columns and cannot easily account for the highly radiogenic $^{187}Os/^{188}Os$ values, which indicate a very long residence time of the source prior to extraction of melt.

Alkali picrites in the North China Craton with similarly unusual high Zr/Ti composition to those described from the Wirrda Well prospect (Huang et al., 2016) were interpreted by Gao et al. (2008) as the products of partial melting of a pyroxenitic mantle source. They envisaged a process of delamination of (mafic) lower crust and lithospheric mantle followed by reaction of melts derived from the foundered lower crust with peridotitic lithosphere to form the pyroxenitic source. In contrast, we do not advocate foundering of dense lower crust in the case of the Gawler Craton and Curnamona Province, because there is no evidence in the available data for complete replacement of lithospheric mantle up to the Moho level. Rather, we suggest that pyroxenitic sources with crust-like geochemical signatures (from prior subduction-related metasomatism) were partially melted at midlithospheric levels and speculate that this melting was driven by foundering of only lowermost lithospheric mantle as compared to lower crust.

An additional possible source of mantle melts are the descending *drips* of foundered lithospheric mantle, which theoretically could result in hydrous alkali-rich melts from the volatile-rich drip itself or from *wet* melting of adjacent asthenosphere (Ducea et al., 2013; Elkins-Tanton & Foulger, 2005; Murray et al., 2015). The extent to which such processes may have contributed to magmatism in the Gawler Craton and Curnamona Province is unknown but could be tested with further petrogenetic modeling and radiogenic (Nd, Sr, and Os) isotope analysis of mafic igneous rocks.

In the period 1,575–1,550 Ma to present, much of the region underwent a thermal decline and *cratonization*, although some regions were affected by a resumption of compressional deformation and possibly exhumation (e.g., parts of northern Gawler Craton such as the Coober Pedy Ridge, and northern Curnamona Province including the Mt Painter Inlier). It is possible that the Cariewerloo Basin, including the Pandurra Formation, which has zircon maximum depositional ages of ~1,590 Ma and was lithified by ~1,450 Ma (Cherry et al., 2017; Fanning & Link, 2003), was a consequence of the subsidence related to cooling that followed lithospheric thinning/foundering.

5.3. Relationship Between IOCG Deposit Formation, Mantle Metasomatism, and Lithospheric Architecture

Neodymium isotope studies of the Olympic Dam deposit have shown that up to ~30% of the Nd in the REE-rich deposit was likely contributed from isotopically primitive (mantle-derived) sources such as mafic/ultramafic igneous rocks and/or magmas (Johnson & McCulloch, 1995). As Cu contents are positively correlated with Nd concentration, and mafic/ultramafic dykes are common in the deposit, Johnson and McCulloch (1995) suggested that a significant proportion of the Cu in the deposit was also sourced from mantle-derived rocks or magmas. Further Nd isotope studies on *barren* and weakly Cu-Au mineralized iron oxide-rich hydrothermal systems in the Olympic Dam region revealed that these hydrothermal systems lack the same primitive Nd isotope compositions as occur at the Olympic Dam deposit, implying lower contributions of Nd (and by implication other metals) from mantle-derived sources (Skirrow et al., 2007). Thus, it was concluded that a key factor in the formation of the giant Olympic Dam Cu-U-Au deposit was the availability of mantle-derived sources of Cu, either via leaching of mafic volcanic rocks or mafic/ultramafic intrusive rocks (Haynes et al., 1995; Skirrow et al., 2007), or via a direct contribution of mafic/ultramafic magma-derived magmatic-hydrothermal fluids (Campbell et al., 1998; Johnson & McCulloch, 1995). Empirically, however, there is a general lack of major hydrothermal ore deposits directly associated with the crystallization of mafic or ultramafic magmas as compared with intermediate to felsic magmas (e.g., Hedenquist, 2005). Moreover, leaching of the ore metals as well as Fe and K is recorded in regional Na ± Ca alteration zones within mafic and felsic igneous rocks and metasedimentary rocks in the Gawler Craton, Curnamona Province (Bastrakov et al., 2007; Clark et al., 2005) and in other IOCG provinces (e.g., Cloncurry, Oliver et al., 2004). For these reasons we prefer a model involving leaching of at least some Cu from mantle-derived rocks (see also Bastrakov et al., 2007; Skirrow, 2010; Skirrow et al., 2007). It should be noted that the results of Johnson and McCulloch (1995) are also permissive of some Nd contributions from other, less primitive, source rocks. This would also appear to be essential for the U in the deposit (the largest U resource in the world; BHP Annual Report, 2017, www.bhp.com), which was probably sourced from felsic igneous rocks in the region (Hitzman & Valenta, 2005).

We propose that the major IOCG deposits formed close to the eastern boundary of the zone of mantle metasomatism and lithospheric removal in the Gawler Craton (Figures 11 and 12). Thus, the locations of the major IOCG deposits are interpreted to be directly linked to the observed lithospheric architecture.

However, the relationship between mantle metasomatism, mafic/ultramafic magmatism and IOCG ore formation is suggested to be indirect, whereby the tectonic setting favorable for the production of large volumes of mafic-ultramafic melts and their emplacement in the midcrust to upper crust was also favorable for the generation of fluids capable of leaching metals from host rocks including the crystallized mafic/ultramafic magmas, felsic igneous rocks, and metasedimentary rocks. In our model, the large-volume mafic-ultramafic melts were largely the result of remelting of previously metasomatized lithospheric mantle, driven by foundering of lithospheric mantle. This same process resulted in a switch from compressional to extensional tectonism, in a setting inboard of a continental margin. Emplacement of felsic and mafic magmas in the upper crust may have resulted in very high geothermal gradients, capable of driving deep fluid circulation and heating of Fe-rich brines (Hayward & Skirrow, 2010; Skirrow et al., 2007). We suggest that this setting was also favorable for the generation and flow of surface-derived (i.e., groundwater, lake water, or seawater) warm hydrothermal waters (Bastrakov et al., 2007; Haynes et al., 1995). The most significant IOCG deposits are proposed to have formed where these two contrasting fluids mixed or overprinted one-another (Bastrakov et al., 2007; Haynes et al., 1995; Skirrow, 2010). Mixing of shallow-crustal and deeper-crustal fluid reservoirs is facilitated during changes in regional kinematics, such as a switch from compression to extension (Oliver et al., 2004). Such a switch in tectonic style for the Gawler Craton and Curnamona Province, described herein, therefore is a favorable setting for fluid mixing and major IOCG deposit formation.

Richards and Mumin (2013) argued that a subset of IOCG deposits they termed *magmatic-hydrothermal IOCG* deposits (in which they included the Olympic Dam deposit) formed in tectonic settings similar to those of the postsubduction sub-type of porphyry copper deposits. Although we agree on the postsubduction distal arc or back-arc setting for the Olympic Dam deposit, nonmagmatic fluids were probably crucial in its formation (Bastrakov et al., 2007; Haynes et al., 1995; Oreskes & Einaudi, 1992), and no porphyry type Cu deposits have so far been identified in the Gawler Craton or Curnamona Province. The recycling of chalcophile elements such as Cu and Au from metasomatized mantle or MASH zones into later mafic/ultramafic melts via processes of remelting, and thence into IOCG deposits (Groves et al., 2010; Richards & Mumin, 2013), seems plausible, notwithstanding the limitations in the transfer of ore metals from mafic/ultramafic magmas directly to the IOCG deposits by aqueous magmatic-hydrothermal fluids, noted earlier. Groves et al. (2010) suggested an intermediate step involving volatile and metal transfer from mafic/ultramafic magmas into felsic magmas, and thence to the IOCG deposits. In our view, however, the available evidence, including Nd isotope tracing of metal sources, is most consistent with an indirect transfer of metals via leaching of mafic/ultramafic igneous rocks, themselves derived from metasomatized mantle, together with leaching of felsic and metase-dimentary rocks. More generally, Groves et al. (2010) proposed a genetic link between major IOCG deposits globally and mafic (in places alkaline) magmas derived by mantle plume-induced partial melting of metaso-matized lithospheric mantle. This model is partly supported by the results of our study of the Gawler Craton and Curnamona Province. With regard to southern Australia we differ, however, in our interpretation of both the driver of partial melting of lithospheric mantle and the tectonic setting in which this melting occurred.

6. Conclusions and Exploration Implications

Integration of 3-D mantle geophysical (seismic tomographic and MT), igneous geochemical, isotopic (Nd, Os, Hf), and geological data for the Gawler Craton and Curnamona Province has revealed new features in the lithospheric architecture that bear upon the geodynamic, tectonic, and IOCG ore-forming systems evolution and prospectivity of the region. The most important findings are as follows.

A previously identified zone of high electrical conductivity (resistivity <10 ohm.m) with top at ~100–150 km depths in lithospheric mantle of the central and eastern Gawler Craton is largely hosted by a broader zone with low shear wave velocity ($\lesssim$4.6 km/s) relative to that of typical Archean-Proterozoic lithospheric mantle.

Most of the known major IOCG deposits including the Olympic Dam, Prominent Hill, and Carrapateena deposits occur above or along the northeastern and northern margin of the lithospheric mantle-hosted high-conductivity zone where it coincides with a horizontal gradient in S wave velocity (Vsh and Vsv) at depths of ~100–150 km. This velocity gradient extends from the central-northern Gawler Craton eastward beneath the central Curnamona Province and is at least partly followed by zones of enhanced electrical conductivity in the lithospheric mantle. Empirically, we predict that the upper crust above this gradient could represent a broad zone of favorable prospectivity for major IOCG deposits.

The broad low-Vsh and low-Vsv zone (≲4.6 km/s) in the central and southern Gawler Craton is interpreted to represent refertilized and metasomatized lithospheric mantle that was previously melt-depleted, based on consideration of published seismic velocity properties of mantle minerals and rocks together with garnet compositions in kimberlite-hosted xenoliths. The deeper part of the low-Vsh zone with high electrical conductivity is interpreted to comprise fertile peridotite including minerals characterized by high Vp/Vs (>1.80) and high electrical conductivities such as water-bearing relatively Fe-rich olivine, clinohumite, water-rich almandine-rich garnet, and/or phlogopite.

A MLD has been identified by the presence of a sheet-like zone of relatively low Vp (and low Vp/Vsh), with base at ~130 km depth. The vertical gradient in Vp correlates with sharp changes in the compositions of mantle-derived garnet xenocrysts carried by Permian and Jurassic kimberlites in the region. We interpret the low-Vp layer to contain locally high proportions of orthopyroxene from an early (Archean?) metasomatic event.

Our preferred geodynamic and tectonic model involves foundering of gravitationally destabilized lowermost, previously refertilized, metasomatized, and rheologically weak lithospheric mantle beneath the central and southern Gawler Craton and southern Curnamona Province at ~1,610–1,575 Ma. A likely trigger for lithospheric destabilization was accretion/collision at a former continental margin represented in part by the ~1,620–1,610 Ma St Peter Suite igneous rocks. Removal of lithospheric mantle resulted in decompressional melting of ascending asthenosphere and thence partial melting of previously metasomatized lithospheric mantle that was newly exposed to the convecting mantle and its ascending partial melts. The range of observed magma types in the ~1,595–1,575 Ma Hiltaba Suite and comagmatic GRV is viewed as a consequence of the varied lithospheric mantle, asthenospheric, and crustal sources.

The Olympic Dam deposit and other IOCG deposits in the region are interpreted to have formed at ~1,595–1,575 Ma in a postsubduction, synorogenic to postorogenic setting, distal from a continental margin during a tectonic switch from compression to extension. This setting differs from previously proposed mantle plume-related and back-arc settings.

The Gawler Craton is considered to represent an unusual example of an Archean-Proterozoic craton that has undergone partial destruction of its lithospheric root. This process may have been fundamental in the development of the craton's world-class IOCG deposits because it was conducive for the generation and emplacement of large volumes of mafic and felsic igneous rocks in the upper crust, guided by prior trans-lithospheric weaknesses such as boundaries between cratonic blocks. The proposed setting provided favorable upper crustal conditions for the generation of Cu-Au-U-rich ore fluids via leaching of mafic and felsic igneous and other rocks, thence mixing with a second, surface-derived, hydrothermal fluid.

Appendix A: Data Sets

A1. Seismic Velocity Data

Shear-wave or *S* wave velocity (Vs) data from the mantle component of the Australian Seismological Reference Model (AuSREM; Kennett et al., 2013) were interrogated within a GOCAD® 3-D model to derive velocity isosurfaces, cross sections, and plan sections. We utilized both the horizontal (Vsh) and vertical (Vsv) velocity components of Vs in the AuSREM mantle model to better understand spatial variations in anisotropy (e.g., Figure 6b). The Vsh component has been used in many of the figures (including those showing Vp/Vsh) because the spatial relationships between Vsh, electrical conductivity, geochemistry, and geology are clearer than, or similar to, those using the Vsv component. The AuSREM mantle model is gridded with a 0.5° cell size and enables resolution of bodies of anomalous *S* wave velocity measuring as small as 250 km horizontally and 30 km vertically (Kennett et al., 2013).

Sun and Kennett (2016) presented a 3-D *P* wave model of Australia, which was derived from inversion of Pn travel time data and used the AuSREM data set as a starting model. The horizontal resolution of the *P* wave model is 3° × 3° or better for western and central Australia (including the current study area) and 4° × 4° for eastern Australia, and the *P* wave inversion extends to depths of 180 km (Sun & Kennett, 2016). We created a new model of Vp/Vs for the continent using the vertical and horizontal components of the AuSREM mantle *S* wave data set with the *P* wave model of Sun and Kennett (2016). An extract from the Vp/Vsh model is shown in Figure 3.

Two data sets for the depth of the LAB were utilized, from Kennett et al. (2013) and Czarnota et al. (2013). The LAB of Kennett et al. (2013) in the region of interest in South Australia corresponds quite closely to the lower bound of the lithosphere-asthenosphere transition zone described by Kennett et al. (2017).

Selected data from the seismic tomography models are presented for the study area in the 3-D model in the supplementary information.

A2. MT Data

Long-period MT data from Thiel and Heinson (2013) for the Gawler Craton, which were incorporated into the South Australian Geophysical Reference Model (van der Wielen et al., 2016), were integrated into a 3-D model in the present study (see the supporting information, and extract in Figure 3). The spacings of MT stations ranged from ~10 to ~80 km, with significant parts of the survey acquired at ~50 km spacing. Details of acquisition, processing, and modeling are described by Thiel and Heinson (2013). MT data also have been acquired for the region to the east of the Gawler Craton including the Adelaide Rift Complex and the Curnamona Province (Robertson et al., 2016). We have utilized available images of the results for the region east of the Gawler Craton, where the station spacing is generally ~50 km.

A3. Neodymium, Osmium, and Hafnium Isotope Data

Two primary neodymium isotope data sets were utilized. The first, used to map variations in neodymium isotope model ages of felsic igneous rocks (whole-rock samples), is based on the Australian continental study of Champion (2013). This data set was supplemented by data from Stewart and Foden (2003); the combined data were regridded, and two-stage depleted mantle (2DM) model ages calculated at 1,500 Ma to produce a new *residence age* map for the Gawler Craton and Curnamona Province. This map is a representation of the variations in (Nd model) ages of the sources of felsic igneous rocks as they would have appeared at 1,500 Ma. The additional data utilized in this study provide an improved spatial resolution of model age variations compared to the data set of Champion (2013).

A second neodymium isotope data set, for 1,600–1,575 Ma mafic igneous rocks in the Gawler Craton and Curnamona Province, was compiled from published sources. Due to the sparsity of samples, gridding and mapping of isotopic compositions were not attempted; however, individual epsilon-Nd values were utilized to compare with other data sets.

Osmium ($^{187}Os/^{188}Os$) and hafnium whole-rock isotope data are available for a small number of Hiltaba Suite-age and GRV mafic igneous rocks (Pankhurst et al., 2013).

A4. Whole-Rock Mafic Igneous Geochemical Data

Whole-rock major and trace element geochemical data were compiled from published sources, focused on 1,600–1,575 Ma mafic and alkaline igneous rocks from the Gawler Craton and Curnamona Province. Sources include Budd (2006), Wade (2012, and references therein), Wade et al. (2012), Huang et al. (2016), Government of South Australia SARIG database, and references therein (data extracted 2017 from https://map.sarig.sa.gov.au/), and Geoscience Australia (2007, OZCHEM database and references therein, http://www.ga.gov.au/metadata-gateway/metadata/record/65464/). These data include outcrop and drill hole samples of mafic volcanic and intrusive rocks, and alkaline intrusive rocks. Although the data set includes a variety of analytical methods, detection limits, and ranges of elements analyzed, there are sufficient data of acceptable quality to enable reconnaissance comparisons of different mafic igneous units. The whole-rock geochemical data and sources are available in the supporting information.

A5. Mantle Xenocryst and Xenolith Data

Kimberlitic and related alkaline rocks that intruded parts of the southern and southeastern Gawler Craton and adjacent Neoproterozoic Adelaide Rift Complex in the Permian and Jurassic carried a range of mantle-derived materials including rare diamond, garnet xenocrysts, and mantle xenoliths (Cooper & Morris, 2012; Gaul et al., 2003; Tappert et al., 2011). Although the garnet-clinopyroxene-orthopyroxene-spinel dominated assemblages of the xenoliths lack olivine, the presence of serpentine and compositions of other silicates

led Tappert et al. (2011) to conclude that the mantle source rocks were olivine-bearing, and described the mantle xenoliths as *garnet peridotite*. Moreover, Foden et al. (2016) noted the presence of eclogite (garnet pyroxenite) xenoliths in some kimberlitic intrusions. Xenocrystic pyrope garnet compositions were investigated by Gaul et al. (2003) and Tappert et al. (2011); clinopyroxene, orthopyroxene and chromite were also analyzed by Tappert et al. (2011). These data were used by Gaul et al. (2003) and Tappert et al. (2011) to calculate geotherms (Permian and Jurassic) and also to infer the compositions of coexisting minerals (e.g., Mg/(Mg + Fe) of olivine) and the nature of metasomatism in the lithospheric mantle beneath the Gawler Craton and younger terranes to the east. We have drawn on the results of these studies to compare the mantle compositions inferred from mantle xenocrysts/xenoliths with the spatial variations in seismic velocity and electrical conductivity in the lithospheric mantle.

A6. Geochronological and Geological Data

The geophysical, geochemical, and isotopic data sets described above have been integrated with information on the geology and evolution of the Gawler Craton and Curnamona Province, and their IOCG and gold mineral systems. Key sources of geological and geochronological data include Cowley (2008), Ferris et al. (2002), Fitzherbert and Downes (2017), Fraser et al. (2007), Hand et al. (2007), Reid (2017), Reid and Hand (2012), Skirrow (2010), and Skirrow et al. (2002, 2007).

References

Abers, G. A., & Hacker, B. R. (2016). A MATLAB toolbox and Excel workbook for calculating the densities, seismic wave speeds, and major element composition of minerals and rocks at pressure and temperature. *Geochemistry, Geophysics, Geosystems*, *17*, 616–624. https://doi.org/10.1002/2015GC006171

Afonso, J. C., Ranalli, G., Fernàndez, M., Griffin, W. L., O'Reilly, S. Y., & Faul, U. (2010). On the Vp/Vs–Mg# correlation in mantle peridotites: Implications for the identification of thermal and compositional anomalies in the upper mantle. *Earth and Planetary Science Letters*, *289*(3–4), 606–618.

Allen, S. R., McPhie, J., Ferris, G., & Simpson, C. (2008). Evolution and architecture of a large felsic igneous province in western Laurentia: The 1.6 Ga Gawler Range Volcanics, South Australia. *Journal of Volcanology and Geothermal Research*, *172*(1–2), 132–147.

Arndt, N. T., Coltice, N., Helmstaedt, H., & Gregoire, M. (2009). Origin of Archean subcontinental lithospheric mantle: Some petrological constraints. *Lithos*, *109*(1–2), 61–71.

Babeyko, A. Y., Sobolev, S. V., Trumbull, R. B., Oncken, O., & Lavier, L. L. (2002). Numerical models of crustal scale convection and partial melting beneath the Altiplano–Puna plateau. *Earth and Planetary Science Letters*, *199*(3–4), 373–388.

Bao, X., Eaton, D. W., & Guest, B. (2014). Plateau uplift in western Canada caused by lithospheric delamination along a craton edge. *Nature Geoscience*, *7*(11), 830–833.

Bastrakov, E. N., Skirrow, R. G., & Davidson, G. J. (2007). Fluid evolution and origins of iron oxide Cu-Au prospects in the Olympic Dam district, Gawler craton, South Australia. *Economic Geology*, *102*(8), 1415–1440.

Beck, S. L., Zandt, G., Ward, K. M., & Scire, A. (2015). Multiple styles and scales of lithospheric foundering beneath the Puna Plateau, central Andes. In P. G. de Celles, M. N. Ducea, B. Carrapa, & P. A. Kapp (Eds.), *Geodynamics of a Cordilleran Orogenic System: The Central Andes of Argentina and Northern Chile. Memoir of the Geological Society of America 212*, (pp. 43–60). America: The Geological Society of America.

Begg, G. C., Hronsky, J. A., Arndt, N. T., Griffin, W. L., O'Reilly, S. Y., & Hayward, N. (2010). Lithospheric, cratonic, and geodynamic setting of Ni-Cu-PGE sulfide deposits. *Economic Geology*, *105*(6), 1057–1070.

Behn, M. D., & Kelemen, P. B. (2006). Stability of arc lower crust: Insights from the Talkeetna arc section, south central Alaska, and the seismic structure of modern arcs. *Journal of Geophysical Research*, *111*, B11207. https://doi.org/10.1029/2006JB004327

Belperio, A., Flint, R., & Freeman, H. (2007). Prominent Hill: A hematite-dominated, iron oxide copper-gold system. *Economic Geology*, *102*(8), 1499–1510.

Betts, P. G., Giles, D., Foden, J., Schaefer, B. F., Mark, G., Pankhurst, M. J., et al. (2009). Mesoproterozoic plume-modified orogenesis in eastern Precambrian Australia. *Tectonics*, *28*, TC3006. https://doi.org/10.1029/2008TC002325

Betts, P. G., Mason, W. G., & Moresi, L. (2012). The influence of a mantle plume head on the dynamics of a retreating subduction zone. *Geology*, *40*(8), 739–742.

Bird, P. (1979). Continental delamination and the Colorado Plateau. *Journal of Geophysical Research*, *84*(B13), 7561–7571. https://doi.org/10.1029/JB084iB13p07561

Bowden, B., Fraser, G., Davidson, G. J., Meffre, S., Skirrow, R. G., Bull, S., & Thompson, J. (2017). Age constraints on the hydrothermal history of the Prominent Hill iron oxide copper-gold deposit, South Australia. *Mineralium Deposita*, *52*(6), 863–881.

Budd, A. R. (2006). The Tarcoola Goldfield of the Central Gawler Gold Province, and the Hiltaba Association Granites, Gawler Craton, South Australia. Unpublished PhD. Thesis, Australian National University.

Budd, A. R., & Skirrow, R. G. (2007). The nature and origin of gold deposits of the Tarcoola goldfield and implications for the Central Gawler gold province, South Australia. *Economic Geology*, *102*(8), 1541–1563.

Campbell, I. H., Compston, D. M., Richards, J. P., Johnson, J. P., & Kent, A. J. R. (1998). Review of the application of isotopic studies to the genesis of Cu-Au mineralisation at Olympic Dam and Au mineralisation at Porgera, the Tennant Creek district and Yilgarn Craton. *Australian Journal of Earth Sciences*, *45*(2), 201–218.

Carr, L. K., Korsch, R. J., Holzschuh, J., Costelloe, R. D., Meixner, A. J., Matthews, C and Godsmark, B. (2010). Geological interpretation of seismic reflection lines 08GA-C1 and 09TE-01: Arrowie Basin, South Australia. In: Korsch, R.J. and Kositcin, N., South Australian Seismic and MT Workshop 2010, Extended Abstracts. *Geoscience Australia Record* 2010/10, 54–65.

Chalot-Prat, F., & Girbacea, R. (2000). Partial delamination of continental mantle lithosphere, uplift-related crust–mantle decoupling, volcanism and basin formation: A new model for the Pliocene–Quaternary evolution of the southern East-Carpathians, Romania. *Tectonophysics*, *327*(1–2), 83–107.

Champion, D. C. (2013). Neodymium depleted mantle model age map of Australia: Explanatory notes and user guide. *Geoscience Australia Record* 2013/044. http://dx.doi.org/10.11636

Chen, M., Niu, F., Tromp, J., Lenardic, A., Lee, C. T. A., Cao, W., & Ribeiro, J. (2017). Lithospheric foundering and underthrusting imaged beneath Tibet. *Nature Communications*, *8*, 15659. https://doi.org/10.1038/ncomms15659

Cherry, A. R., McPhie, J., Kamenetsky, V. S., Ehrig, K., Keeling, J. L., Kamenetsky, M. B., et al. (2017). Linking Olympic Dam and the Cariewerloo Basin: Was a sedimentary basin involved in formation of the world's largest uranium deposit? *Precambrian Research*, *300*, 168–180.

Ciobanu, C. L., Wade, B. P., Cook, N. J., Mumm, A. S., & Giles, D. (2013). Uranium-bearing hematite from the Olympic Dam Cu–U–Au deposit, South Australia: A geochemical tracer and reconnaissance Pb–Pb geochronometer. *Precambrian Research*, *238*, 129–147.

Clark, C., Mumm, A. S., & Faure, K. (2005). Timing and nature of fluid flow and alteration during Mesoproterozoic shear zone formation, Olary Domain, South Australia. *Journal of Metamorphic Geology*, *23*(3), 147–164.

Conor, C. C. H., Raymond, O., Baker, T., Teale, G., Say, P., & Lowe, G. (2010). Alteration and mineralisation in the Moonta-Wallaroo copper-gold mining field region, Olympic Domain, South Australia. In: Porter, T. M. (Editor). *Hydrothermal iron oxide copper-gold & related deposits: A global perspective*, *3*, 4.

Cooper, S. A. & Morris, B. J. (2012). A review of kimberlites and related rocks in South Australia. *Department for Manufacturing, Innovation, Trade, Resources and Energy. Report Book*, 2012/00006.

Cowley, W. M. (compiler) (2008). Solid geology of South Australia: Archaean to Early Mesoproterozoic time slice map. *Geological Survey of South Australia*. Retrieved from https://sarigbasis.pir.sa.gov.au/WebtopEw/ws/samref/sarig1/wcir/Record?r=0&m=1&w=catno=2038279

Creaser, R. A. (1996). Petrogenesis of a Mesoproterozoic quartz latite-granitoid suite from the Roxby Downs area, South Australia. *Precambrian Research*, *79*(3–4), 371–394.

Curtis, S., Wade, C., & Reid, A. (2018). Sedimentary basin formation associated with a silicic large igneous province: Stratigraphy and provenance of the Mesoproterozoic Roopena Basin, Gawler Range Volcanics. *Australian Journal of Earth Sciences*, 1–17.

Czarnota, K., Hoggard, M. J., White, N., & Winterbourne, J. (2013). Spatial and temporal patterns of Cenozoic dynamic topography around Australia. *Geochemistry, Geophysics, Geosystems*, *14*, 634–658. https://doi.org/10.1029/2012GC004392

Czarnota, K., Roberts, G. G., White, N. J., & Fishwick, S. (2014). Spatial and temporal patterns of Australian dynamic topography from River Profile Modeling. *Journal of Geophysical Research: Solid Earth*, *119*, 1384–1424. https://doi.org/10.1002/2013JB010436

Dai, L., & Karato, S. I. (2009). Electrical conductivity of pyrope-rich garnet at high temperature and high pressure. *Physics of the Earth and Planetary Interiors*, *176*(1–2), 83–88.

Djomani, Y. H. P., O'Reilly, S. Y., Griffin, W. L., & Morgan, P. (2001). The density structure of subcontinental lithosphere through time. *Earth and Planetary Science Letters*, *184*(3–4), 605–621.

Ducea, M. N., Seclaman, A. C., Murray, K. E., Jianu, D., & Schoenbohm, L. M. (2013). Mantle-drip magmatism beneath the Altiplano-Puna plateau, central Andes. *Geology*, *41*(8), 915–918.

Duncan, R. J., Stein, H. J., Evans, K. A., Hitzman, M. W., Nelson, E. P., & Kirwin, D. J. (2011). A new geochronological framework for mineralization and alteration in the Selwyn-Mount Dore corridor, Eastern fold belt, Mount Isa inlier, Australia: Genetic implications for iron oxide copper-gold deposits. *Economic Geology*, *106*(2), 169–192.

Eeken, T., Goes, S., Pedersen, H. A., Arndt, N. T., & Bouilhol, P. (2018). Seismic evidence for depth-dependent metasomatism in cratons. *Earth and Planetary Science Letters*, *491*, 148–159.

Elkins-Tanton, L. T., & Foulger, G. R. (2005). Continental magmatism caused by lithospheric delamination. *Special Papers, Geological Society of America*, *388*, 449–461.

Ernst, R. E. (2014). *Large igneous provinces*. Cambridge: Cambridge University Press.

Fadil, A., Vernant, P., McClusky, S., Reilinger, R., Gomez, F., Sari, D. B., et al. (2006). Active tectonics of the western Mediterranean: Geodetic evidence for rollback of a delaminated subcontinental lithospheric slab beneath the Rif Mountains, Morocco. *Geology*, *34*(7), 529–532.

Fanning, C. M. (1990). Single grain U-Pb zircon dating of two tuffaceous horizons from Wilgena #1. PRISE (Australian National University) Report G 7519/88 (unpublished).

Fanning, C. M., & Link, P. K. (2003). *Detrital zircon provenance of the Mesoproterozoic Pandurra Formation, South Australia: Gawler Craton—Zircon population and implications for the Belt Supergroup, Abstracts with Programs*, (Vol. 35, p. 465). Seattle: Geological Society of America.

Ferris, G. M., & Schwarz, M. P. (2003). Proterozoic gold province of the central Gawler Craton. *MESA Journal*, *30*, 4–12.

Ferris, G. M., Schwarz, M. P., & Heithersay, P. (2002). The geological framework, distribution and controls of Fe-Oxide Cu-Au mineralisation in the Gawler Craton, South Australia. Part I—Geological and tectonic framework. In: Porter, T. M. (Editor). *Hydrothermal iron oxide copper-gold and related deposits: A global perspective*, *2*, 9–31.

Fitzherbert, J. A., & Downes, P. M. (2017). Curnamona Province—Geological history and mineral systems. In G. N. Phillips (Ed.), *Australian ore deposits, monograph*, (Vol. 32, pp. 635–640). Melbourne: The Australasian Institute of Mining and Metallurgy.

Foden, J., Stewart, K., Tregeagle, J. and Ross, A. (2016). The 1595Ma Gawler Range Volcanics: Petrogenesis of a silicic large igneous province. Abstracts, 35th International Geological Congress, Cape Town, South Africa. *American Geosciences Institute*, https://www.americangeosciences.org/geotimes/35th-igc-full-text-abstracts-available.

Forbes, C. J., Giles, D., Betts, P. G., Weinberg, R., & Kinny, P. D. (2007). Dating prograde amphibolite and granulite facies metamorphism using in situ monazite U-Pb SHRIMP analysis. *The Journal of Geology*, *115*(6), 691–705.

Ford, H. A., Fischer, K. M., Abt, D. L., Rychert, C. A., & Elkins-Tanton, L. T. (2010). The lithosphere–asthenosphere boundary and cratonic lithospheric layering beneath Australia from Sp wave imaging. *Earth and Planetary Science Letters*, *300*(3–4), 299–310.

Fraser, G., McAvaney, S., Neumann, N., Szpunar, M., & Reid, A. (2010). Discovery of early Mesoarchean crust in the eastern Gawler Craton, South Australia. *Precambrian Research*, *179*(1–4), 1–21.

Fraser, G. L., & Lyons, P. (2006). Timing of Mesoproterozoic tectonic activity in the northwestern Gawler Craton constrained by $^{40}Ar/^{39}Ar$ geochronology. *Precambrian Research*, *151*(3–4), 160–184.

Fraser, G. L., Skirrow, R. G., Schmidt-Mumm, A., & Holm, O. (2007). Mesoproterozoic gold in the central Gawler craton, South Australia: Geology, alteration, fluids, and timing. *Economic Geology*, *102*(8), 1511–1539.

Gao, S., Rudnick, R. L., Xu, W. L., Yuan, H. L., Liu, Y. S., Walker, R. J., et al. (2008). Recycling deep cratonic lithosphere and generation of intraplate magmatism in the North China Craton. *Earth and Planetary Science Letters*, *270*(1), 41–53.

Gaul, O. F., O'Reilly, S. Y. and Griffin, W. L. (2003). Lithosphere structure and evolution in southeastern Australia. *Special Papers, Geological Society of America*, 185–202.

Giles, C. W. (1988). Petrogenesis of the Proterozoic Gawler Range Volcanics, South Australia. *Precambrian Research*, *40*, 407–427.

Gorczyk, W., & Vogt, K. (2015). Tectonics and melting in intra-continental settings. *Gondwana Research*, *27*(1), 196–208.

Groves, D. I., Bierlein, F. P., Meinert, L. D., & Hitzman, M. W. (2010). Iron oxide copper-gold (IOCG) deposits through Earth history: Implications for origin, lithospheric setting, and distinction from other epigenetic iron oxide deposits. *Economic Geology*, *105*(3), 641–654.

Hacker, B. R., & Abers, G. A. (2012). Subduction Factory 5: Unusually low Poisson's ratios in subduction zones from elastic anisotropy of peridotite. *Journal of Geophysical Research*, *117*, B06308. https://doi.org/10.1029/2012JB009187

Hand, M., Reid, A., & Jagodzinski, L. (2007). Tectonic framework and evolution of the Gawler craton, southern Australia. *Economic Geology*, *102*(8), 1377–1395.

Havlin, C., Parmentier, E. M., & Hirth, G. (2013). Dike propagation driven by melt accumulation at the lithosphere–asthenosphere boundary. *Earth and Planetary Science Letters*, *376*, 20–28.

Haynes, D. W., Cross, K. C., Bills, R. T., & Reed, M. H. (1995). Olympic Dam ore genesis; a fluid-mixing model. *Economic Geology*, *90*(2), 281–307.

Hayward, N., & Skirrow, R. G. (2010). Geodynamic setting and controls on iron oxide Cu-Au (±U) ore in the Gawler craton, South Australia. In: Porter, T. M. (Editor). *Hydrothermal iron oxide copper-gold and related deposits: A global perspective*, *3*, 105–131.

Hedenquist, J. W. (Ed.) (2005). *Economic Geology: One Hundredth Anniversary Volume: 1905-2005* (Vol. 1905). Society of Economic Geologists Incorporated.

Hitzman, M. W. (2000). Iron oxide-Cu-Au deposits: What, where, when, and why. In: Porter, T. M. (Editor). *Hydrothermal iron oxide copper-gold and related deposits: A global perspective*, *1*, 9–25.

Hitzman, M. W., Oreskes, N., & Einaudi, M. T. (1992). Geological characteristics and tectonic setting of Proterozoic iron oxide (Cu ± U ± Au ± REE) deposits. *Precambrian Research*, *58*(1–4), 241–287.

Hitzman, M. W., & Valenta, R. K. (2005). Uranium in iron oxide-copper-gold (IOCG) systems. *Economic Geology*, *100*(8), 1657–1661.

Hoatson, D. M., Sun, S. S., Duggan, M. B., Davies, M. B., Daly, S. J., & Purvis, A. C. (2005). Late Archean Lake Harris komatiite, central Gawler craton, South Australia: geologic setting and geochemistry. *Economic Geology*, *100*(2), 349–374.

Hoernle, K., White, J. V., van den Bogaard, P., Hauff, F., Coombs, D. S., Werner, R., et al. (2006). Cenozoic intraplate volcanism on New Zealand: Upwelling induced by lithospheric removal. *Earth and Planetary Science Letters*, *248*(1), 350–367.

Houseman, G., & Molnar, P. (2001). Mechanisms of lithospheric rejuvenation associated with continental orogeny. *Geological Society, London, Special Publications*, *184*(1), 13–38.

Houseman, G. A., McKenzie, D. P., & Molnar, P. (1981). Convective instability of a thickened boundary layer and its relevance for the thermal evolution of continental convergent belts. *Journal of Geophysical Research*, *86*(B7), 6115–6132. https://doi.org/10.1029/JB086iB07p06115

Hu, J., Liu, L., Faccenda, M., Zhou, Q., Fischer, K. M., Marshak, S., & Lundstrom, C. (2018). Modification of the Western Gondwana craton by plume-lithosphere interaction. *Nature Geoscience*, *11*, 203–210.

Huang, Q., Kamenetsky, V. S., Ehrig, K., McPhie, J., Kamenetsky, M., Cross, K., et al. (2016). Olivine-phyric basalt in the Mesoproterozoic Gawler silicic large igneous province, South Australia: Examples at the Olympic Dam Iron Oxide Cu–U–Au–Ag deposit and other localities. *Precambrian Research*, *281*, 185–199.

Jagodzinski, E., Reid, A., Crowley, J., McAvaney, S. and Wade, C. (2016). Precise zircon U-Pb dating of Mesoproterozoic silicic large igneous province: the Gawler Range Volcanics and Benagerie Volcanic Suite, South Australia. Abstracts, Australian Earth Science Convention, 2016. Geological Society of Australia.

Johnson, J. P., & Cross, K. C. (1995). U-Pb geochronological constraints on the genesis of the Olympic Dam Cu-U-Au-Ag deposit, South Australia. *Economic Geology*, *90*(5), 1046–1063.

Johnson, J. P., & McCulloch, M. T. (1995). Sources of mineralising fluids for the Olympic Dam deposit (South Australia): Sm-Nd isotopic constraints. *Chemical Geology*, *121*(1–4), 177–199.

Jones, A. G. (2016). Proton conduction and hydrogen diffusion in olivine: an attempt to reconcile laboratory and field observations and implications for the role of grain boundary diffusion in enhancing electrical conductivity. *Physics and Chemistry of Minerals*, *43*, 237–265.

Jones, A. G., Evans, R. L., & Eaton, D. W. (2009). Velocity–conductivity relationships for mantle mineral assemblages in Archean cratonic lithosphere based on a review of laboratory data and Hashin–Shtrikman extremal bounds. *Lithos*, *109*(1–2), 131–143.

Kay, R. W., & Kay, S. M. (1993). Delamination and delamination magmatism. *Tectonophysics*, *219*(1–3), 177–189.

Kennett, B. L., Fichtner, A., Fishwick, S., & Yoshizawa, K. (2013). Australian seismological reference model (AuSREM): Mantle component. *Geophysical Journal International*, *192*(2), 871–887.

Kennett, B. L. N., Salmon, M., Saygin, E., & Group, A. W. (2011). AusMoho: the variation of Moho depth in Australia. *Geophysical Journal International*, *187*(2), 946–958.

Kennett, B. L. N., Yoshizawa, K., & Furumura, T. (2017). Interactions of multi-scale heterogeneity in the lithosphere: Australia. *Tectonophysics*, *717*, 193–213.

Kopylova, M. G., Lo, J., & Christensen, N. I. (2004). Petrological constraints on seismic properties of the Slave upper mantle (Northern Canada). *Lithos*, *77*(1–4), 493–510.

Krystopowicz, N. J., & Currie, C. A. (2013). Crustal eclogitization and lithosphere delamination in orogens. *Earth and Planetary Science Letters*, *361*, 195–207.

Levander, A., Schmandt, B., Miller, M. S., Liu, K., Karlstrom, K. E., Crow, R. S., et al. (2011). Continuing Colorado plateau uplift by delamination-style convective lithospheric downwelling. *Nature*, *472*(7344), 461.

Li, Y., Yang, X., Yu, J. H., & Cai, Y. F. (2016). Unusually high electrical conductivity of phlogopite: the possible role of fluorine and geophysical implications. *Contributions to Mineralogy and Petrology*, *171*(4), 37.

Li, Z.-X. A., Lee, C.-T., Peslier, A. H., Lenardic, A., & Mackwell, S. J. (2008). Water contents in mantle xenoliths from the Colorado Plateau and vicinity: Implications for the mantle rheology and hydration-induced thinning of continental lithosphere. *Journal of Geophysical Research*, *113*, B09210. https://doi.org/10.1029/2007JB005540

Lustrino, M. (2005). How the delamination and detachment of lower crust can influence basaltic magmatism. *Earth-Science Reviews*, *72*(1–2), 21–38.

McAvaney, S. & Wade, C. E. (2015). Stratigraphy of the lower Gawler Range Volcanics in the Roopena area, northeastern Eyre Peninsula. *Department of State Development, South Australia*, Report Book 2015/00021.

McPhie, J., Kamenetsky, V. S., Chambefort, I., Ehrig, K., & Green, N. (2011). Origin of the supergiant Olympic Dam Cu-U-Au-Ag deposit, South Australia: Was a sedimentary basin involved? *Geology*, *39*(8), 795–798.

McPhie, J., Orth, K., Kamenetsky, V., Kamenetsky, M., & Ehrig, K. (2016). Characteristics, origin and significance of Mesoproterozoic bedded clastic facies at the Olympic Dam Cu–U–Au–Ag deposit, South Australia. *Precambrian Research*, *276*, 85–100.

Morency, C., Doin, M. P., & Dumoulin, C. (2002). Convective destabilization of a thickened continental lithosphere. *Earth and Planetary Science Letters*, *202*(2), 303–320.

Murray, K. E., Ducea, M. N., & Schoenbohm, L. (2015). Foundering-driven lithospheric melting: The source of central Andean mafic lavas on the Puna Plateau (22 S–27 S). In: de Celles, P. G., Ducea, M. N., Carrapa, B. and Kapp, P. A. (Eds), Geodynamics of a Cordilleran Orogenic System: The Central Andes of Argentina and Northern Chile. *Geological Society of America Memoirs*, *212*, 139–166.

Oliver, N. H., Cleverley, J. S., Mark, G., Pollard, P. J., Fu, B., Marshall, L. J., et al. (2004). Modeling the role of sodic alteration in the genesis of iron oxide-copper-gold deposits, eastern Mount Isa block, Australia. *Economic Geology*, 99(6), 1145–1176.

Ootes, L., Snyder, D., Davis, W. J., Acosta-Góngora, P., Corriveau, L., Mumin, A. H., et al. (2017). A Paleoproterozoic Andean-type iron oxide copper-gold environment, the Great Bear magmatic zone, Northwest Canada. *Ore Geology Reviews*, 81, 123–139.

Oreskes, N., & Einaudi, M. T. (1992). Origin of hydrothermal fluids at Olympic Dam; preliminary results from fluid inclusions and stable isotopes. *Economic Geology*, 87(1), 64–90.

Pankhurst, M. J., Schaefer, B. F., Turner, S. P., Argles, T., & Wade, C. E. (2013). The source of A-type magmas in two contrasting settings: U–Pb, Lu–Hf and Re–Os isotopic constraints. *Chemical Geology*, 351, 175–194.

Pearce, J. A. (2008). Geochemical fingerprinting of oceanic basalts with applications to ophiolite classification and the search for Archean oceanic crust. *Lithos*, 100(1–4), 14–48.

Pearce, J. A. (2014). Immobile element fingerprinting of ophiolites. *Elements*, 10(2), 101–108.

Plank, T., & Forsyth, D. W. (2016). Thermal structure and melting conditions in the mantle beneath the Basin and Range province from seismology and petrology. *Geochemistry, Geophysics, Geosystems*, 17, 1312–1338. https://doi.org/10.1002/2015GC006205

Pommier, A., & Le-Trong, E. (2011). "SIGMELTS": A web portal for electrical conductivity calculations in geosciences. *Computers & Geosciences*, 37(9), 1450–1459.

Rader, E., Emry, E., Schmerr, N., Frost, D., Cheng, C., Menard, J., et al. (2015). Characterization and petrological constraints of the midlithospheric discontinuity. *Geochemistry, Geophysics, Geosystems*, 16, 3484–3504. https://doi.org/10.1002/2015GC005943

Reeve, J. S., Cross, K. C., Smith, R. N., & Oreskes, N. (1990). Olympic Dam copper-uranium-gold-silver deposit. In: Geology of the mineral deposits of Australia and Papua New Guinea. *Australasian Intsitute of Mining and Metallurgy, Monograph*, 14, 1009–1035.

Reid, A., Smith, R. N., Baker, T., Jagodzinski, E. A., Selby, D., Gregory, C. J., & Skirrow, R. G. (2013). Re-Os dating of molybdenite within hematite breccias from the Vulcan Cu-Au prospect, Olympic Cu-Au province, South Australia. *Economic Geology*, 108(4), 883–894.

Reid, A. J. (2017). Geology and metallogeny of the Gawler Craton. In G. N. Phillips (Ed.), *Australian Ore Deposits, Monograph*, (Vol. 32, pp. 589–594). Melbourne: The Australasian Institute of Mining and Metallurgy.

Reid, A. J., & Hand, M. (2012). Mesoarchean to mesoproterozoic evolution of the southern Gawler Craton, South Australia. *Episodes*, 35(1), 216–225.

Reid, A. J., & Jagodzinski, E. A. (2013). PACE Geochronology: Extending our understanding of the age and context of mineral systems. *MESA Journal*, 69, 58–65.

Richards, J. P., & Mumin, A. H. (2013). Magmatic-hydrothermal processes within an evolving Earth: Iron oxide-copper-gold and porphyry Cu ±Mo±Au deposits. *Geology*, 41(7), 767–770.

Robertson, K., Heinson, G., & Thiel, S. (2016). Lithospheric reworking at the Proterozoic–Phanerozoic transition of Australia imaged using AusLAMP Magnetotelluric data. *Earth and Planetary Science Letters*, 452, 27–35.

Rossi, G., Abers, G. A., Rondenay, S., & Christensen, D. H. (2006). Unusual mantle Poisson's ratio, subduction, and crustal structure in central Alaska. *Journal of Geophysical Research*, 111, B09311. https://doi.org/10.1029/2005JB003956

Rutherford, L. (2006). Developing a tectonic framework for the southern CurnamonaCu-Au province: geochemical and radiogenic isotope applications. Unpublished Ph.D. thesis, The University of Adelaide, South Australia.

Rutherford, L., Burtt, A. C., Barovich, K. M., Hand, M., & Foden, J. (2007). Billeroo North alkaline magmatic complex: Geology and economic significance. Department of State Development, South Australia, Adelaide. *MESA Journal*, 45, 33–39.

Schlegel, T. U., & Heinrich, C. A. (2015). Lithology and hydrothermal alteration control the distribution of copper grade in the Prominent Hill iron oxide-copper-gold deposit (Gawler craton, South Australia). *Economic Geology*, 110(8), 1953–1994.

Schott, B., & Schmeling, H. (1998). Delamination and detachment of a lithospheric root. *Tectonophysics*, 296(3–4), 225–247.

Schurr, B., Rietbrock, A., Asch, G., Kind, R., & Oncken, O. (2006). Evidence for lithospheric detachment in the central Andes from local earthquake tomography. *Tectonophysics*, 415(1–4), 203–223.

Selway, K. (2014). On the causes of electrical conductivity anomalies in tectonically stable lithosphere. *Surveys in Geophysics*, 35(1), 219–257.

Shervais, J. W. (1982). Ti-V plots and the petrogenesis of modern and ophiolitic lavas. *Earth and Planetary Science Letters*, 59(1), 101–118.

Sillitoe, R. H. (2003). Iron oxide-copper-gold deposits: an Andean view. *Mineralium Deposita*, 38(7), 787–812.

Skirrow, R. G. (1999). Proterozoic Cu-Au-Fe mineral systems in Australia: Filtering key components in exploration models. In C. J. Stanley (Ed.), *Mineral deposits: Processes to processing*, (pp. 1361–1364). Rotterdam: Balkema.

Skirrow, R. G. (2010). Hematite-group IOCG ± U systems: Tectonic settings, hydrothermal characteristics, and Cu-Au and U mineralizing processes. In: Corriveau, L. & Mumin, H. (Editors), Exploring for iron oxide copper-gold deposits: Canada and global analogues. *Geological Association of Canada, Short Course Notes*, 20, 39–59.

Skirrow, R. G. (2016). Lithospheric and tectonic settings of IOCG systems in Australia. Abstracts, 35th International Geological Congress, 27 August – 4 September 2016, Cape Town, South Africa.

Skirrow, R. G., Ashley, P. M., McNaughton, N. J., & Suzuki, K. (2000). Time–space framework of Cu–Au–(Mo) and regional alteration systems in the Curnamona Province. *Australian Geological Survey Organisation Record*, 10, 83–86.

Skirrow, R. G., Bastrakov, E., Davidson, G. J., Raymond, O., & Heithersay, P. (2002). Geological framework, distribution and controls of Fe-oxide Cu-Au deposits in the Gawler craton. Part II. Alteration and mineralization. In: Porter, T. M. (Editor), Hydrothermal iron oxide copper-gold and related deposits: Adelaide, South Australia. *Porter GeoConsultancy Publishing*, 2, 33–47.

Skirrow, R. G., Bastrakov, E. N., Barovich, K., Fraser, G. L., Creaser, R. A., Fanning, C. M., et al. (2007). Timing of iron oxide Cu-Au-(U) hydrothermal activity and Nd isotope constraints on metal sources in the Gawler craton, South Australia. *Economic Geology*, 102(8), 1441–1470.

Snyder, D. B. (2008). Stacked uppermost mantle layers within the Slave craton of NW Canada as defined by anisotropic seismic discontinuities. *Tectonics*, 27, TC4006. https://doi.org/10.1029/2007TC002132

Snyder, D. B., Hillier, M. J., Kjarsgaard, B. A., de Kemp, E. A., & Craven, J. A. (2014). Lithospheric architecture of the Slave craton, northwest Canada, as determined from an interdisciplinary 3-D model. *Geochemistry, Geophysics, Geosystems*, 15, 1895–1910. https://doi.org/10.1002/2013GC005168

Snyder, D. B., Humphreys, E., & Pearson, D. G. (2017). Construction and destruction of some North American cratons. *Tectonophysics*, 694, 464–485.

Stewart, K. (1994). High temperature felsic volcanism and the role of mantle magmas in Proterozoic crustal growth: the Gawler Range Volcanic Province. Unpublished Ph.D. thesis, The University of Adelaide, South Australia, 214p.

Stewart, K. and Foden, J. (2003). Mesoproterozoic granites of South Australia. *South Australia Department of Primary Industries and Resources, Report Book*, 2003/00015. https://sarigbasis.pir.sa.gov.au/WebtopEw/ws/samref/sarig1/image/DDD/RB200300015.pdf

Sun, W., & Kennett, B. L. N. (2016). Uppermost mantle structure of the Australian continent from Pn traveltime tomography. *Journal of Geophysical Research - Solid Earth*, 121, 2004–2019. https://doi.org/10.1002/2015JB012597

Swain, G., Barovich, K., Hand, M., Ferris, G., & Schwarz, M. (2008). Petrogenesis of the St Peter Suite, southern Australia: Arc magmatism and Proterozoic crustal growth of the South Australian Craton. *Precambrian Research*, *166*(1–4), 283–296.

Tappert, R., Foden, J., Muehlenbachs, K., & Wills, K. (2011). Garnet peridotite xenoliths and xenocrysts from the Monk Hill Kimberlite, South Australia: Insights into the lithospheric mantle beneath the Adelaide Fold Belt. *Journal of Petrology*, *52*(10), 1965–1986.

Thiel, S., & Heinson, G. (2013). Electrical conductors in Archean mantle—Result of plume interaction? *Geophysical Research Letters*, *40*, 2947–2952. https://doi.org/10.1002/grl.50486

Thiel, S., Robertson, K. and Heinson, G. (2017). Evolving 3D resistivity models of the South Australian lithosphere derived from AusLAMP MT. Abstracts, *American Geophysical Union*, Fall Meeting, 11–15 December 2017, New Orleans, USA.

Thybo, H., & Artemieva, I. M. (2013). Moho and magmatic underplating in continental lithosphere. *Tectonophysics*, *609*, 605–619.

Van der Wielen, S. E., Thiel, S., Goodwin, J., Lane, R., Chopping, R., Fabris, A. J., Keeping, T., Keeling, J. and Giles, D. (2016). South Australian Geophysical Reference Model, GOCAD® version 1 (3D digital dataset). Geoscience Data Package 00037. Department of State Development, South Australia, Adelaide. http://dsd-gdp.s3.amazonaws.com/GDP00037.zip

Van Wijk, J. W., Baldridge, W. S., Van Hunen, J., Goes, S., Aster, R., Coblentz, D. D., et al. (2010). Small-scale convection at the edge of the Colorado Plateau: Implications for topography, magmatism, and evolution of Proterozoic lithosphere. *Geology*, *38*(7), 611–614.

Wade, C. E. (2012). Geochemistry of pre-1570 Ma mafic magmatism within South Australia: implications for possible tectonic settings and timing of major mineralisation events in South Australia. Report Book 2012/00019, *Department of State Development*, *South Australia*, Adelaide.

Wade, C. E., Reid, A. J., Wingate, M. T., Jagodzinski, E. A., & Barovich, K. (2012). Geochemistry and geochronology of the c. 1585 Ma Benagerie Volcanic Suite, southern Australia: Relationship to the Gawler Range Volcanics and implications for the petrogenesis of a Mesoproterozoic silicic large igneous province. *Precambrian Research*, *206*, 17–35.

Wagner, L. S., Anderson, M. L., Jackson, J. M., Beck, S. L., & Zandt, G. (2008). Seismic evidence for orthopyroxene enrichment in the continental lithosphere. *Geology*, *36*(12), 935–938.

Williams, P. J., & Skirrow, R. G. (2000). Overview of iron oxide-copper-gold deposits in the Curnamona Province and Cloncurry district (Eastern Mount Isa Block), Australia. In: Porter, T. M. (Editor). *Hydrothermal iron oxide copper-gold and related deposits: A global perspective*, *1*, 105–122.

Wingate, M. T., Campbell, I. H., Compston, W., & Gibson, G. M. (1998). Ion microprobe U–Pb ages for Neoproterozoic basaltic magmatism in south-central Australia and implications for the breakup of Rodinia. *Precambrian Research*, *87*(3–4), 135–159.

Worthington, J. R., Hacker, B. R., & Zandt, G. (2013). Distinguishing eclogite from peridotite: EBSD-based calculations of seismic velocities. *Geophysical Journal International*, *193*(1), 489–505.

Yang, X., & McCammon, C. (2012). Fe^{3+}-rich augite and high electrical conductivity in the deep lithosphere. *Geology*, *40*(2), 131–134.

Zhao, J. X., McCulloch, M. T., & Korsch, R. J. (1994). Characterisation of a plume-related ~800 Ma magmatic event and its implications for basin formation in central-southern Australia. *Earth and Planetary Science Letters*, *121*(3–4), 349–367.